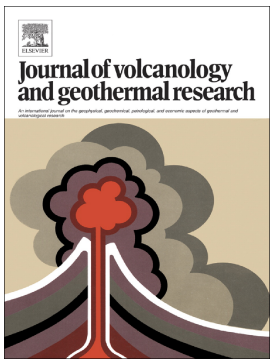

Volcanism and hydrothermalism on a hotspot–influenced ridge: Comparing Reykjanes Peninsula and Reykjanes Ridge, Iceland

Dominik Pałgan, Colin W. Devey, Isobel A. Yeo

PII: S0377-0273(17)30061-6
DOI: doi:10.1016/j.jvolgeores.2017.10.017
Reference: VOLGEO 6225

To appear in: *Journal of Volcanology and Geothermal Research*

Received date: 27 January 2017
Revised date: 27 October 2017
Accepted date: 28 October 2017

Please cite this article as: Dominik Pałgan, Colin W. Devey, Isobel A. Yeo , Volcanism and hydrothermalism on a hotspot–influenced ridge: Comparing Reykjanes Peninsula and Reykjanes Ridge, Iceland. The address for the corresponding author was captured as affiliation for all authors. Please check if appropriate. Volgeo(2017), doi:10.1016/j.jvolgeores.2017.10.017

Volcanism and hydrothermalism on a hotspot–influenced ridge: Comparing Reykjanes Peninsula and Reykjanes Ridge, Iceland

Dominik Pałgan[1*], Colin W. Devey[1] and Isobel A. Yeo[2]

[1]GEOMAR, Helmholtz Centre for Ocean Research Kiel, Wischhofstr. 1–3, 24148, Kiel, Germany

[2]National Oceanography Centre Southampton, Waterfront Campus, European Way, Southampton SO14 3ZH, United Kingdom

*Corresponding author (dpalgan@geomar.de)

Abstract

Current estimates indicate that the number of high-temperature vents (one of the primary pathways for the heat extraction from the Earth's mantle) – at least 1 per 100 km of axial length – scales with spreading rate and should scale with crustal thickness. But up to present, shallow ridge axes underlain by thick crust show anomalously low incidences of high-temperature activity. Here we compare the Reykjanes Ridge, an abnormally shallow ridge with thick crust and only one high-temperature vent known over 900 km axial length, to the adjacent subaerial Reykjanes Peninsula (RP), which is characterized by high-temperature geothermal sites confined to four volcanic systems transected by fissure swarms with young (Holocene) volcanic activity, multiple faults, cracks and fissures, and continuous seismic activity. New high-resolution bathymetry (gridded at 60 m) of the Reykjanes Ridge between 62°30'N and 63°30'N shows seven Axial Volcanic Ridges (AVR) that, based on their morphology, geometry and tectonic regime, are analogues for the volcanic systems and fissure swarms on land. We investigate in detail the volcano-tectonic features of all mapped AVRs and show that they do not fit with the previously suggested 4-stage evolution model for AVR construction. Instead, we suggest that AVR morphology reflects the robust or weak melt supply to the system and two (or more) eruption mechanisms may co-exist on one AVR (in contrast to 4-stage evolution model). Our interpretations indicate that, unlike on the Reykjanes Peninsula, faults on and around AVRs do not cluster in orientation domains but all are subparallel to the overall strike of AVRs (orthogonal to spreading direction). High abundance of seamounts shows that the region centered at 62°47'N and 25°04'W (between AVR-5 and -6) is volcanically robust while the highest fault density implies that AVR-1 and southern part of AVR-6 rather undergo period of melt starvation. Based on our observations and interpretations we expect all of the AVRs on Reykjanes Ridge to be hydrothermally active but morphological and hydrographic settings of this ridge may cause hydrothermal

plumes to be quickly dispersed and diluted due to exposure to strong bottom currents. Therefore, combined CTD and autonomous vehicles surveys are probably the most efficient methods for hydrothermal exploration along the Reykjanes Ridge.

Key words: Reykjanes Peninsula, Reykjanes Ridge, Mid-Atlantic Ridge, Axial Volcanic Ridge, Hydrothermal activity, Steinahóll Vent Field

1 Introduction

Early estimates of Baker and German (2004) and later of Beaulieu et al. (2015) predict that the incidence of high-temperature hydrothermal venting along slow-spreading ridges (full spreading rate 20–40mm/yr) should be between 1–2 vent fields per 100 km of the ridge axis and be correlated with spreading rate. On hotspot–influenced sections of ridge, higher incidences are expected due to higher magma (and hence heat) fluxes. This effect is observed on, for example, the Mid-Atlantic Ridge (MAR) south of the Azores, where 1 vent field every ~25–30 km (German et al., 1996) is present, high for its ca. 25 mm/yr full-spreading rate. In contrast, on the Reykjanes Ridge (RR, Fig. 1), which lies close to the Iceland hotspot, only one system (the Steinahóll Vent Field, German et al., 1994) has to-date been discovered along 900 km of axis. This contrasts starkly with the adjacent, subaerial Reykjanes Peninsula (RP) which has six high-temperature geothermal areas (they are – from west to east – Reykjanes, Eldvörp, Svartsengi, Krísuvík-Trölladyngja, Brennisteinsfjöll and Hengill (with three wellfields – Nesjavellir, Hellisheidi and Hveragerdi)) along ~80 km of axis (e.g., Torfason, 2003; Arnórsson et al., 2008). It is unclear if this apparent paucity of vents along the RR is because they are not present (and the ridge-axis is being cooled by mechanisms other than high-temperature venting) or if they have just not yet been detected. Beside the implications for the thermal balance of such shallow ridges, determining how and where the Reykjanes Ridge loses its heat also has implications for marine mineral prospecting and chemosynthetic biogeography of the northern Atlantic.

The subaerial Reykjanes Peninsula (Fig. 2) provides a unique opportunity to observe directly the interaction between volcanic, tectonic and hydrothermal processes on the divergent plate boundary. It shows many similarities in terms of geomorphology, mechanisms of volcanic activity, tectonism and seismicity to the RR. Conducting fieldwork on land is, of course, easier than in the deep ocean, allowing us to map and assess the geological setting of hydrothermalism much more quickly and easily than would be possible using research vessels. Hence, extrapolation of controls of venting on the RP combined with interpretation of

high-resolution ship-based bathymetry of the RR can helps us better predict locations of new hydrothermal systems on this hotspot-influenced ridge.

In this paper we use high resolution ship-based bathymetry (gridded at 60 m) of a 100 km section of the Reykjanes Ridge between 62°30'N and 63°30'N to investigate the volcano-tectonic setting of the plate boundary. We focus on the volcanic status and evolution of seven Axial Volcanic Ridges (AVRs), which have previously been suggested to be off-shore equivalents of the on-land volcanic systems on the RP (Jakobsson et al., 1978; Murton and Parson, 1993; Höskuldsson et al., 2007) . Our observations and interpretations, combined with direct observations from the subaerial Reykjanes Peninsula, can help us better understand off-shore hydrothermal systems and cooling mechanisms along shallow, abnormally thick and hotspot-influenced mid-ocean ridges.

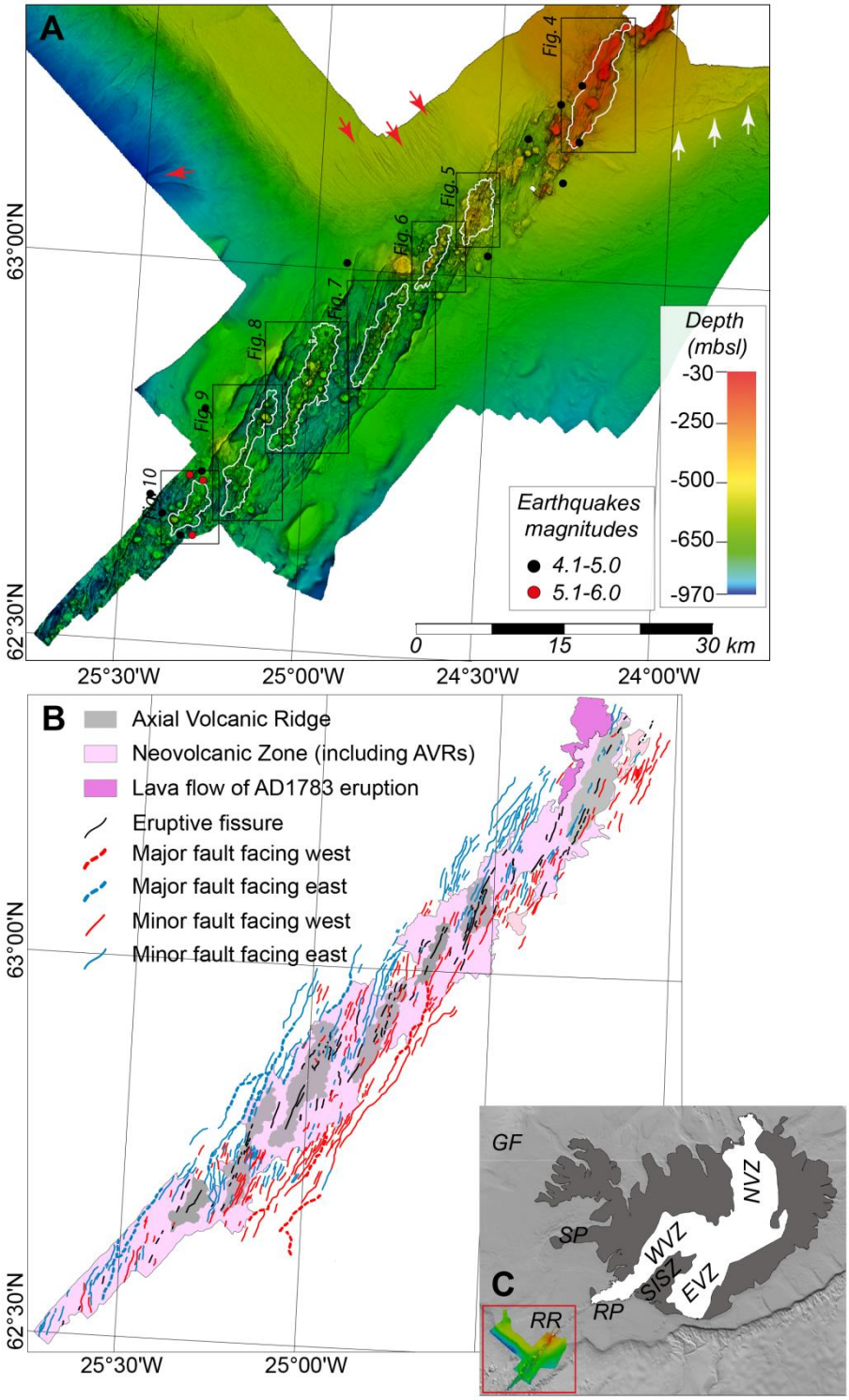

Fig. 1 (A) Multibeam bathymetry of the Reykjanes Ridge between 62°30'N and 63°30'N, gridded at 60 m. White lines outline the seven Axial Volcanic Ridges mapped in this area. Black and red dots indicate the relocated earthquake epicenters for 1950-2015 from the International Seismological Center (ISC) (Engdahl et al., 1998)**. White arrows indicate braided system of moraines while red arrows show erosional channels engraved in the sedimented terrain. (B) Simplified geological map of the ridge axis, based on an interpretation of panel A. The neovolcanic zone appears as rough volcanic terrain comprising hummocky terrain, eruptive fissures and circular edifices (locally piling up and constructing Axial Volcanic Ridges) and hosts the majority of the present volcanic activity. Circular seamounts are shown in more detail in figures in section 4.3. (C) Overview of the working area with main volcanic and seismic zones on Iceland. RR: Reykjanes Ridge (our working area); RP: Reykjanes Peninsula; SP: Snæfellsnes Peninsula; GF: Greenland-Faroes Ridge; SISZ: South-Iceland Seismic Zone; WVZ: Western Volcanic Zone; EVZ: Easter Volcanic Zone; NVZ: Northern Volcanic Zone; KR: Kolbeinsey Ridge.**

2 Datasets and methods

The Digital Elevation Model (DEM) of the Reykjanes Peninsular used in this study is a smoothed, accurately relocated iteration of data collected during the 2000 Shuttle Radar Topography Mission (SRTM) re-worked by Aleksandr Yashin (*pers. comm.*) and has a resolution of 100 m. The ship-based multibeam bathymetry of the RR between 62°30'N and 63°30'N was collected by the Marine Research Institute (MIR) in Reykjavik (www.hafro.is) on board R/V Árni Friðriksson during the cruise A8–2006 in summer 2006 using the onboard Simrad EM 300 multibeam echosounder. The data were gridded at 60 m resolution using the QPS Fledermaus and DMagic software. The maps presented here and all the interpretations are based on this data using a combination of shaded relief and the terrain texture shader (TTS) techniques, the latter developed by Brown (2010). The TTS enhances the presentation of DEMs by increasing contrast and textural detail (even when the elevation changes abruptly or where the boundaries between features have low relief) and eliminating the concept of illumination direction (Brown, 2010). The combination of shaded relief and TTS techniques has become a standard procedure to analyze and display bathymetric data and it has been used in many seafloor environments (e.g., Yeo et al., 2016; Anderson et al., 2016; Augustin et al., 2016). The overall quality and level of detail presented in the figures is limited by the resolution of the available bathymetric data. Acoustic backscatter information from the same survey is presently undergoing re-processing at MIR and is not presented in this study.

The locations of geothermal fields on the RP were taken from Torfason (2003) and our own field observations; the location of the Steinahóll Vent Field on the RR was taken from German et al. (1994) and the InterRidge Vents Database Ver. 3.3. A simplified geological map of the RP, was produced based on a digitized (using ArcMap 10.1) version of the Geological Map of Southwest Iceland produced at a scale of 1:100 000 (Sæmundsson et al., 2010) and maps published in the literature (e.g., Sæmundsson, 1979; Clifton and Schlische, 2003; Pedersen and Grosse, 2014). A geological map of the RR was produced by interpreting the MRI bathymetry. ArcMap 10.1 software was used to measure the geometry of the features and, where possible (when clear boundaries could be defined), calculate minimum eruption volumes.

In the interpretations given below, the term "eruptive fissure" is often used to refer to the sites of the rejuvenated and/or youngest volcanism. From bathymetric data alone there are some clear criteria which allow us to distinguish such fissures from fault blocks. To classify a feature as an eruptive fissure we require them: (1) to be linear or sinuous in shape and laterally continuous, (2) to be ≤ 1 km wide, (3) to form local highs (mostly >20 m above the

surrounding seafloor), (4) to have no significant depth offsets along their length and (5) to have distinct outward-facing slopes on both sides with slope angles between 5° and 28° (shallower than the dip angles of most axial faults). Examples of mapped eruptive fissures are shown in profiles across individual AVRs in figures in section 4.3. Circular edifices (seamounts) were mapped applying the assumptions of Smith and Cann (1990), who classified 'seamount' as an edifice with relief >50 m above the surrounding seafloor, and the descriptive classification based on the morphology and appearance of the seamounts in the bathymetry. The examples of mapped seamounts types are shown in Fig. 2. All seamounts have basal areas >0.1 km^2. Volcanic cones are distinctive edifices with medium-steep slopes (>15° with max. 26°) and sharp-to-dome-shaped summits (Fig. 2A). Cratered volcanoes (Fig. 2B) also have medium-steep slopes generally >15° with a maximum of 29° and a distinctive crater on the summits (from few to 10s of meters deep). Flat-topped volcanoes were divided into three groups based on the characteristics of the summits and named: flat-, coned- and complex-. They generally have more gentle flank slopes (<20°) but some with 26-29° have been observed. Flat-topped volcanoes are circular to oval in shape with well-defined and flattened summits. Examples of flat-, coned- and complex-flat-topped volcanoes are shown in Figs. 2C-E.

In two cases, two generations of AVRs could be distinguished (current and former). Former AVRs are most visible in the topographic profiles and are classified as former AVRs if they (1) are clearly separated from current AVRs by abrupt change in elevation, caused by either inward-facing faults or an intervening deep basins of relatively flat seafloor (see section 4.3), (2) have distinctive positive relief above the surrounding seafloor, and (3) are composed of multiple volcanic edifices (elongated eruptive fissures and circular volcanoes).

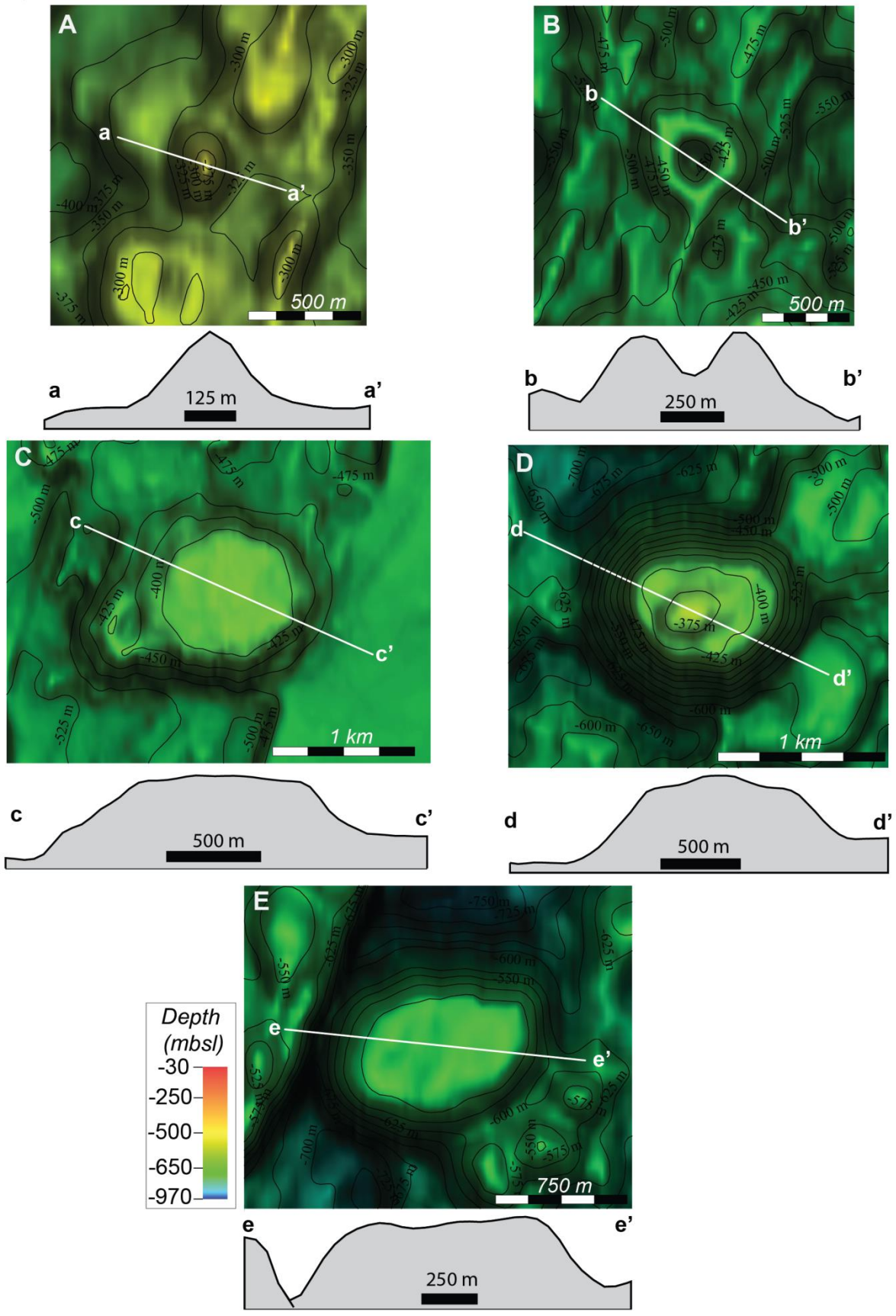

Fig. 2 Detailed bathymetry and profiles of the mapped circular seamounts in the study area. The profiles have 5x vertical exaggeration. (A) Volcanic cone at 63°02'N and 24°35'W; (B) Cratered volcano at 62°57'N and 24°46'W; (C) Flat-topped volcano with flat summit at 62°58'N and 24°38'W; (D) Flat-topped volcano with coned summit at 62°39'N and 25°21'W; (E) Flat-topped volcano with complex summit at 62°37'N and 25°27'W.

3 Geological setting

3.1 Reykjanes Ridge

The Reykjanes Ridge (Fig. 1) is an oblique ~900 km long segment of the northern Mid-Atlantic Ridge (MAR), located between Iceland and the Bight Fracture Zone (57°N), spreading at 1 cm yr^{-1} half rate (e.g., Talwani et al., 1971; Vogt, 1971; Keeton et al., 1997; Searle et al., 1998). It is the longest V-shaped and hotspot-influenced ridge in the world (Ito, 2001) with several unique characteristics. The depth of the ridge axis gradually increases from sea level at the coast to about 2600 m near the Bight Fracture Zone and the axis is characterized by two distinct morphologies. South of 59°N, a median valley typical of slow-spreading ridges (~2.5 km deep and ~15 km wide) is present. It has been suggested that this marks the maximum extent of the Iceland hotspot influence (Talwani et al., 1971; Searle et al., 1994; Peirce et al., 2005; Peirce and Sinha, 2008). North of 59°N, the ridge is characterized by an axial high more typical for intermediate and fast spreading ridges like the Juan de Fuca Ridge or East Pacific Rise (e.g., Talwani et al., 1971). Crustal thicknesses vary from 7–7.5 km near 57°45'N (Sinha et al., 1998), a value typical of oceanic crust uninfluenced by hotspot activity elsewhere in the oceans, to 10.6 km at 62°40'N, 14 km at the tip of the Reykjanes Peninsula and ~21 km at Hengill (Weir et al., 2001). The entire length of the ridge is devoid of first-order offsets (Searle et al., 1994), however, it is constructed of individual en echelon AVRs separated from each other by 3–10 km of flat seafloor (composed of sedimented lava flows), hummocky terrain and sparse volcanic edifices (e.g., Fig. 1A). Each AVR is 20–30 km long, 3–6 km wide and 200–500 m high (Parson et al., 1993; Searle et al., 1998; Keeton et al., 1997). The AVRs trend ~ 015°, oblique to the overall Reykjanes Ridge orientation but almost perpendicular to the spreading direction. Each AVR contains fissure-, conical- and circular cratered-/flat-topped volcanoes up to several kilometers in diameter (Höskuldsson et al., 2007). Searle et al. (1998) mapped 40 AVRs between 58°N and 62°N, while between 63°10'N and Iceland, Höskuldsson et al. (2007) distinguished 10 AVRs and 3 large seamounts. These offshore features are often referred to as morphological analogues of the volcanic systems and fissure swarms observed on the subaerial RP (Fig. 2) (e.g., Jakobsson et al., 1978; Murton and Parson, 1993; Pedersen and Grosse, 2014).

Hydrothermal plume hunting along the RR during the cruise B8 of *R/S Bjarni Sæmundsson* led to the discovery of only one active high-temperature vent field – Steinahóll (63°06'N) (German et al., 1994). This vent site is located in only 250–300 m water depth and has plume properties (high dissolved CH_4, H_2, Si and dissolvable Mn) similar to plumes of some black smokers found along the MAR (German et al., 1994). The location of this vent

site at such shallow depth gives rise to a bubble–rich buoyant plume which was detected by a high frequency (38 kHz) echosounder on board.

Seismic activity along the RR is mostly confined to the ridge axis and neotectonic zone, where it occurs in a band paralleling the Axial Volcanic Ridges (e.g., Fig. 1A). Earthquakes usually occur in swarms and cluster in small (2-5 km circumference) areas and extend ~20 km on each side of the ridge axis (Francis, 1973; Lilwall et al., 1980; Crane et al., 1997; Mochizuki et al., 2000; Goslin et al., 2005). Events with magnitudes higher than 4 are detectable teleseismically with high precision due to the relocation procedure introduced by Engdahl et al. (1998) and are listed, along with epicenter locations, by the International Seismological Centre. Micro-seismicity (M<3), on the other hand, although it may be the dominant mode of seismic activity on the Reykjanes Ridge (Mochizuki et al., 2000) cannot be detected continuously with the present infrastructure. Teleseismic data alone are insufficient to allow a thorough interpretation of the tectonic deformation. According to the International Seismological Centre, in the years 1950 to 2015 only 15 earthquakes with M>4 were detected on the Reykjanes Ridge between 62°30'N and 63°30'N (Fig. 1A), while Mochizuki et al. (2000) recorded >1700 micro-seismic events over a short period of time (~1 month) in 1994 in the area between 62°14'N and 62°51'N.

3.2 Reykjanes Peninsula

The bedrock of the RP comprises basalts of Pleistocene age, covered by later postglacial and historic lava flows (Sigurgeirsson, 2004; Sæmundsson et al., 2010; Johannesson, 2014). Most of the Pleistocene rocks are hyaloclastite ridges, table mountains (tuyas) and basaltic lava flows (Gudmundsson, 1987). The RP has been an active spreading zone for the last 6–7 Ma, when the spreading axis jumped there from its previous location on the Snæfellsnes Peninsula (Sæmundsson, 1979; Johannesson, 1980). The peninsula consists of four highly oblique right stepping en echelon volcanic systems transected by four fissure swarms (Sæmundsson, 1979) marked by tensional fractures, normal and/or strike-slip faults, and volcanic or tectonic fissures (Sæmundsson, 1979; Clifton and Kattenhorn, 2006). From west to east the volcanic systems are: Reykjanes, Krýsuvík, Brennisteinsfjöll, and Hengill (Fig. 3). Each fissure swarm is approximately 15–40 km long, 7–15 km wide and on average strikes N40° E (Sæmundsson, 1979). Each volcanic system is distinctive, both geochemically and spatially and only the Hengill system has developed a central volcano (Sæmundsson, 1979). Between AD950 and AD1240, all four volcanic systems were active, erupting large volumes of lava from elongated fissures. The latest volcanic episode, known as the "Reykjanes Fires" took place between AD1210-1240 (Sigurgeirsson, 2004).

All of the volcanic systems on the RP host geothermal activity (Fig. 3), with 6 high-temperature geothermal fields distinguished over a distance of ~80 km on the peninsula. The **Reykjanes-Eldvörp-Svartsengi geothermal area** is located at the southwest tip of the peninsula and its best-studied **Reykjanes** field covers >1 km^2. The Reykjanes geothermal fluids are undiluted seawater modified chemically by the interaction with the hosting basalts (Arnórsson, 1995), they have a temperature between 250 and 290°C at a depth of a few hundred meters. Many similarities suggest that the Reykjanes geothermal area could be considered an analog for submarine hydrothermal systems although under lower hydrostatic pressure (Fowler et al., 2015; Hannington et al., 2016). The **Krísuvík-Trölladyngja geothermal area** is located in the central part of the peninsula, on the eastern side of the Sveifluháls hyaloclastic ridge and surrounded by multiple fractures of the Krísuvík fissure swarm. Most likely the heat driving geothermal activity here is linked to the historic eruption located just west of the Sveifluháls ridge, with tectonic features providing permeable conduits (Sigurgeirsson, 2004; Sæmundsson et al., 2010). Detailed mapping of hydrothermal alteration suggests that this field covers about 40–60 km^2 (Mawejje, 2007). The main surface activity is visible near the Sveifluháls hyaloclastic ridge area, especially within the fields of Seltún and Main Krýsuvík (Mawejje, 2007; Markússon and Stefánsson, 2011). The **Brennisteinsfjöll geothermal area** is associated with large lava flows of historic and prehistoric ages. Presently, geothermal activity only covers about 0.01 km^2 but evidence of hydrothermal alteration can be observed beyond the boundaries of the lava flows, with evidence of former high-temperature activity found on a fault about 1 km north of the main field (Jónsson, 1978; Maochang, 2001; Sæmundsson et al., 2010). The **Hengill geothermal area** is located at the triple-junction between the Reykjanes Rift Zone, the West Volcanic Zone and the South Iceland Seismic Zone (Arnórsson, 1995; Arnórsson et al., 2008). The high-temperature geothermal field **Nesjavellir** is located where the Hengill fissure swarm intersects the Hengill central volcano (Sæmundsson, 1992; Clifton et al., 2002). Observations and modeling suggest that the magma reservoir beneath this volcano provides the heat to drive geothermal activity with the fissures, faults and dikes of the Hengill fissure swarm providing the permeable flow pathways (Franzson et al., 2010). The temperature of the Nesjavellir geothermal reservoir is >200°C at a depth of 1 km (Haraldsdóttir et al., 2012).

The plate boundary exposed along the RP is characterized by a ~2–5 km wide zone of high seismicity (e.g., Klein et al., 1977; Jakobsdóttir, 2008). The zone trends approximately N80°E in the central part of the peninsula and bends to the south on the western-most part of the peninsula. Seven seismometer stations installed on the RP have been continuously

monitoring seismic activity since 1993 (Stefánsson et al., 1993), recording thousands of earthquakes (Jakobsdóttir, 2008). Older stations distributed across the country have recorded ten earthquakes with M_l greater than 4.1 (Fig. 3) between 1950 and 2015 (based on International Seismic Center (ISC) Bulletin Database and relocated according to Engdahl et al. (1998)).

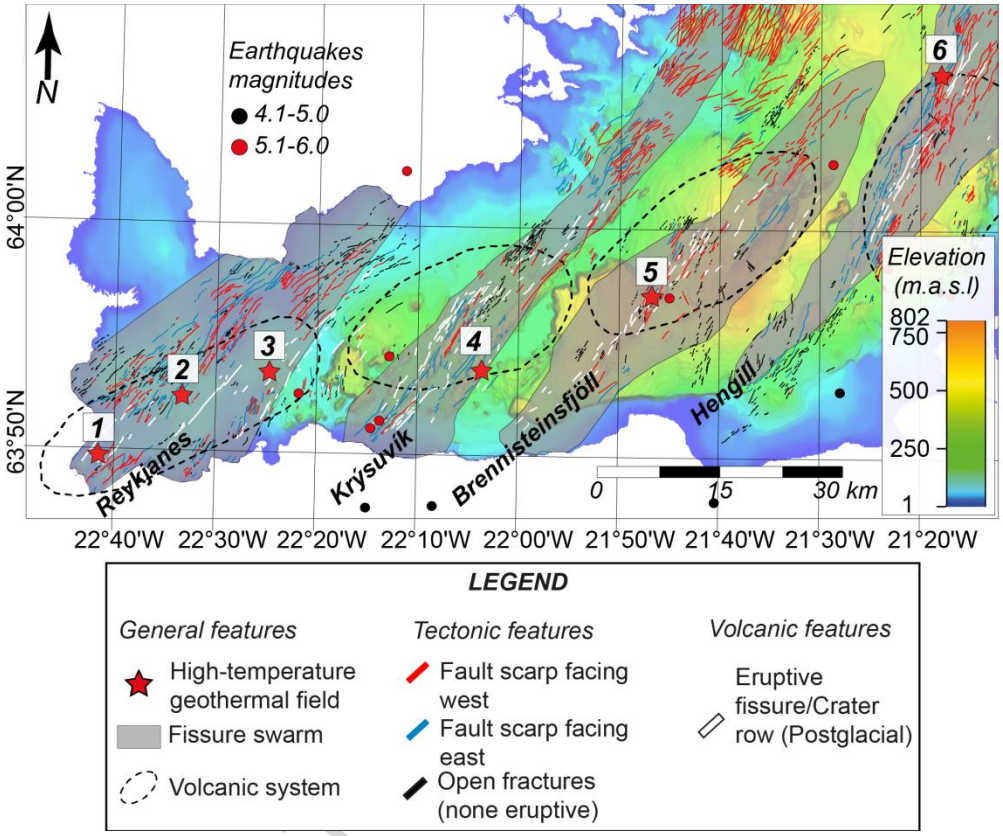

Fig. 3 The simplified topographic (100m DEM) and geological map of the Reykjanes Peninsula (SW Iceland) and associated geothermal areas. The peninsula is a direct, onshore prolongation of the Reykjanes Ridge with four distinctive volcanic systems (from west to east): Reykjanes, Krísuvík, Brennisteinsfjöll and Hengill. All of these volcanic systems are transected by fissure swarms and host high-temperature geothermal activity (from west to east): 1-Reykjanes, 2-Eldvörp, 3-Svartsengi, 4-Krísuvík-Trölladyngja, 5-Brennisteinsfjöll and 6-Hengill. For details on the geological setting of these fields, the reader is referred to the text (Section 3.2) and cited therein literature. The tectonic and volcanic features are based on the digitized map from Sæmundsson et al. (2010). For more detail on the volcanic features, the reader is referred to this map and the literature (Pedersen and Grosse, 2014). Location of volcanic systems taken from Sæmundsson (1979). Locations of geothermal areas according to Arnórsson (1995). Ten major (teleseismically recorded by the International Seismological Center (ISC)) earthquakes (M_l >4) occurred here between 1950 and 2015.

4 Results and interpretations

4.1 General morphology of the spreading axis

The RR axis is bordered by sedimented seafloor. Sediment thicknesses range from <200 m on crust <5 Ma to ~1 km on 10-12 Ma old crust (Ruddiman, 1972). Morphologically, the ridge flanks show smooth terrain interrupted by a few features resembling sediment-covered and tectonized axial volcanoes (e.g., southern part around 25°W, Fig. 1). Our data

confirm that the RR has no first- or second-order offsets in the region studied. The median valley is, on average, 13 km wide and bounded by inward-facing normal faults, the majority of which have throws ranging between 50 and 100 m. This median valley, appearing as rough volcanic terrain constructed by hummocks, eruptive fissures and circular edifices, hosts the majority of the present volcanic and tectonic activity and is interpreted as the neovolcanic zone (Fig. 1B). Most faults (both major and minor with throws ≥100 m and <100 m, respectively) are ridge-parallel and strike NNE-SSW with only a few striking N-S or NNW-SSE (Fig. 1B). Overall, we mapped 244 faults with scarps facing east (nine with throws ≥100 m) and 241 faults with scarps facing west (six with throws ≥100 m). The faults have a wide spectrum of lengths, ranging from ~0.5 to 18.3 km. North of ~63°N, no major faults bounding the ridge axis are visible and the ridge axis forms a prominent high elevated above the surrounding seafloor.

The ridge axis is characterized by multiple linear and usually AVR-parallel volcanic edifices which we interpret as eruptive fissures. They rise from ~20 to even >100 m above the surrounding seafloor and range in length from ~0.2 to 7.0 km. In many cases they connect several circular volcanic edifices (cone-, crater- and/or flat-topped volcanoes) indicating that multiple volcanic edifices may be constructed in a single volcanic event and may be fed by a single underlying dike. Some of the eruptive fissures seem to cut through volcanic edifices, implying they are the youngest features in a given area, possibly of Holocene age; however, with our data we are unable to accurately determine their age.

Following the assumptions of Smith and Cann (1990) and our observations, we mapped 211 seamounts in our study area, of which 41 are volcanic cones (covering areas from 0.07 to 0.83 km^2), 86 cratered volcanoes (covering areas from 0.04 to 5.26 km^2), 42 flat-topped volcanoes with flat summits (covering areas from 0.22 to 3.24 km^2), 20 flat-topped volcanoes with coned summits (covering areas from 0.25 to 5.11 km^2) and 22 flat-topped volcanoes with complex summits (covering areas from 0.63 to 8.93 km^2). The most distinctive seamount along this section of the RR is a complex flat-topped volcano 3.29 km in diameter centered at 63°00'N and 24°45'W. Its summit shows uneven terrain dissected by both east and west facing minor faults, and its highest point reaches ~210 mbsl (Fig. 1A).

4.2 Morphology of the AVRs

The resolution of the bathymetric data allows us to identify an en echelon array of 7 right stepping AVRs between 62°30'N and 63°30'N (Fig. 1A). The main geometric characteristics (including length, width, length/width ratio, covered area, average height above the surrounding seafloor and strike) and observations of these AVRs are summarized in

Table 1. The spacing between the AVRs ranges from 1.5 to 12.3 km and AVR–1/AVR–2 and AVR–3/AVR–4 do not overlap. Otherwise, AVRs overlap over a distance of 1/3 of their length, which is typical for both the northern (Höskuldsson et al., 2007) and southern (Searle et al., 1998) Reykjanes Ridge.

Table 1 Main geometric and morphologic characteristics of the seven AVRs mapped on the Reykjanes Ridge between 62°30'N and 63°30'N. Abbreviations: EF: Eruptive fissures, FTF: Flat-topped volcano-flat summit; FTCS: Flat-topped volcano-conical summit; FTCX: Flat-topped volcano-complex summit; C: Cratered volcano; VC: Volcanic Cone; S: Subsidence structure.

AVR No.	Length (km)	Width (km)	Length/Width ratio	Area (km^2)	Height[1] (m)	Strike	Axial valley width (km)	Volcanic edifices present	Locus of youngest (rejuvenated) volcanism	Youngest volcanic edifices	Seamount density (per 10 km^2)	Generations of AVR	Tectonic deformation	Hydrothermal activity
1	19.7	3.1	6.4	61.0	130	N23.3° E	(?)[1]	EF, FTF, FTCX	Center, South	EF	1	1	+	–
2	10.2	3.1	3.3	28.0	120	N18.4° E	(?)[1]	EF, VC, C, S	Center	EF	4	1	+	+
3	10.3	1.9	5.4	16.7	170	N20.1° E	8.5	EF, VC, C, S	Center	C	5	2	–	–
4	16.7	2.4	7.0	36.1	165	N22.3° E	12.5	EF, VC, C, FTF	Center	EF	4	1	+	–
5	20.0	3.6	5.6	63.5	190	N21.2° E	13.0	EF, VC, C, FTF, FTCS, FTCX	Center	EF	6	1	–	–
6	19.8	2.5	7.9	39.5	180	N18.1° E	11.0	EF, VC, C, FTF, FTCS, FTCX	North, Center	EF/FTF	5	1	+	–
7	8.8	2.4	3.7	20.8	180	N29.1° E	(?)[2]	EF, VC, C, FTF, TCS,	Center, South-West	EF/FTCS	5	2 (?)	–	–

[1]Elevation above the surrounding seafloor; [2]Axial valley not determinable.

4.3 Interpretations

An evolutionary model for the growth and decline of an AVR on the RR has been previously proposed by Murton and Parson (1993) and Parson et al. (1993) based on low-resolution bathymetric information gridded at 100 m. They suggested that each AVR went through a 4-stage life cycle representing arrival, eruption and solidification of a single batch of magma, beginning with (1) eruptions along fissures, followed by the development of (2) conical and then (3) shield-like volcanoes. Their last proposed stage was (4) tectonic dismemberment, which the authors attributed to the consequence of a rapidly decreasing magma supply. Our new bathymetric data allows a more detailed examination of the morphology of the AVRs and shows them to have much more complicated life cycles than Murton and Parson (1993) and Parson et al. (1993) suggest. To illustrate this, an interpretation of the locus and intensity of volcanism on the 7 AVRs mapped here is given below.

AVR-1 (Fig. 4) has the smoothest surface in comparison to the remaining six AVRs which, on first appearances, might suggest that it has experienced much less volcanism in recent times than the others. This conclusion may, however, be erroneous as the surface of AVR-1 has probably been subjected to either (1) intensive glacial and/or fluvio-glacial erosion smoothing the surface, (2) high sedimentation rates masking volcanic surface roughness or (3) intense currents/wave erosion. Glacial and fluvio-glacial erosion seems most likely as, although sedimentary structures (e.g., channels engraved in sediments, see Fig. 1A) are visible on the eastern side of the ridge, we see no such features on top of the AVR and its seamounts. Egloff and Johnson (1979) and later Hubbard et al. (2006) showed through modelling that the ice sheets during the Last Glacial Maximum (LGM) could have extended as far south from Iceland as ~63°10'N, making sub-glacial erosion a viable process on AVR-1. It is also possible that the surface of AVR-1 is additionally subject to currents/waves erosion as some features reach depth of only 40 mbsl. Hey et al. (2003) suggested that current-related erosion reaches depth of 40 mbsl around the area of Vestmannaeyjar off the south coast of Iceland. However, the majority of the AVR-1 is located at depth greater than 100 m. This suggests that some current/wave erosion may be valid here, for example during extreme storm events but is unlikely to be solely responsible for such strong surface smoothing.

The youngest volcanic activity appears to be concentrated in the axial part of the AVR where hummocks, eruptive fissures and smooth/irregular volcanoes are concentrated within a 1.5 km-wide valley bounded by inward-facing minor faults (Fig. 4). Five large smoothed flat-topped volcanoes there seem to be connected by multiple eruptive fissures (Fig. 4A). In three

cases (marked by white-dashed rectangles on Fig. 4B) these eruptive fissures sit on top of the volcanoes implying that they formed most recently. The high level of smoothing and general lack of cross-cutting (e.g., tectonic deformation or overlapping) interactions between features in the northern part makes it very difficult to determine any relative ages. Tectonically dissected volcanic edifices located just E of the 1.5 km wide valley suggest that in the past such volcanoes were building this AVR (Fig. 4B). It seems that, presently, AVR-1 is constructed by eruptions from multiple eruptive fissures located mostly in the central and southern part of the AVR. A large lava flow with what we interpret as prominent lava flow fronts is present NW of the AVR-1 (Fig. 4B). Orientation and shape of these fronts suggest that the flow might have erupted from the hummocky volcanoes located just W of the AVR (centered at 63°17'N and 24°14'W). The lack of tectonic deformation in both the area between the flow and source hummocks, and the lava flow itself suggest it is relatively young, and most likely is a product of a historic eruption in AD1783 (Thorarinsson, 1965). However, with this data set we are unable to determine whether these hummocky volcanoes are of similar age as the eruptive fissures within the median valley and if this lava flow erupted during one or more events. A hummocky terrain located E of the 1.5 km wide valley is isolated from the valley by a prominent east-facing fault and cannot be traced onto the valley floor. This suggests it is an older terrain which was formed before the development of this valley. If the axial valley is located directly at the plate boundary and a 1 cm yr^{-1} half-spreading rate of the RR has not changed significantly over the last few hundred thousand years (an assumption we make for all AVRs), the spreading age (i.e., the age of the outermost structures assuming axisymmetric spreading at constant rate) of the valley is ~17 000 years.

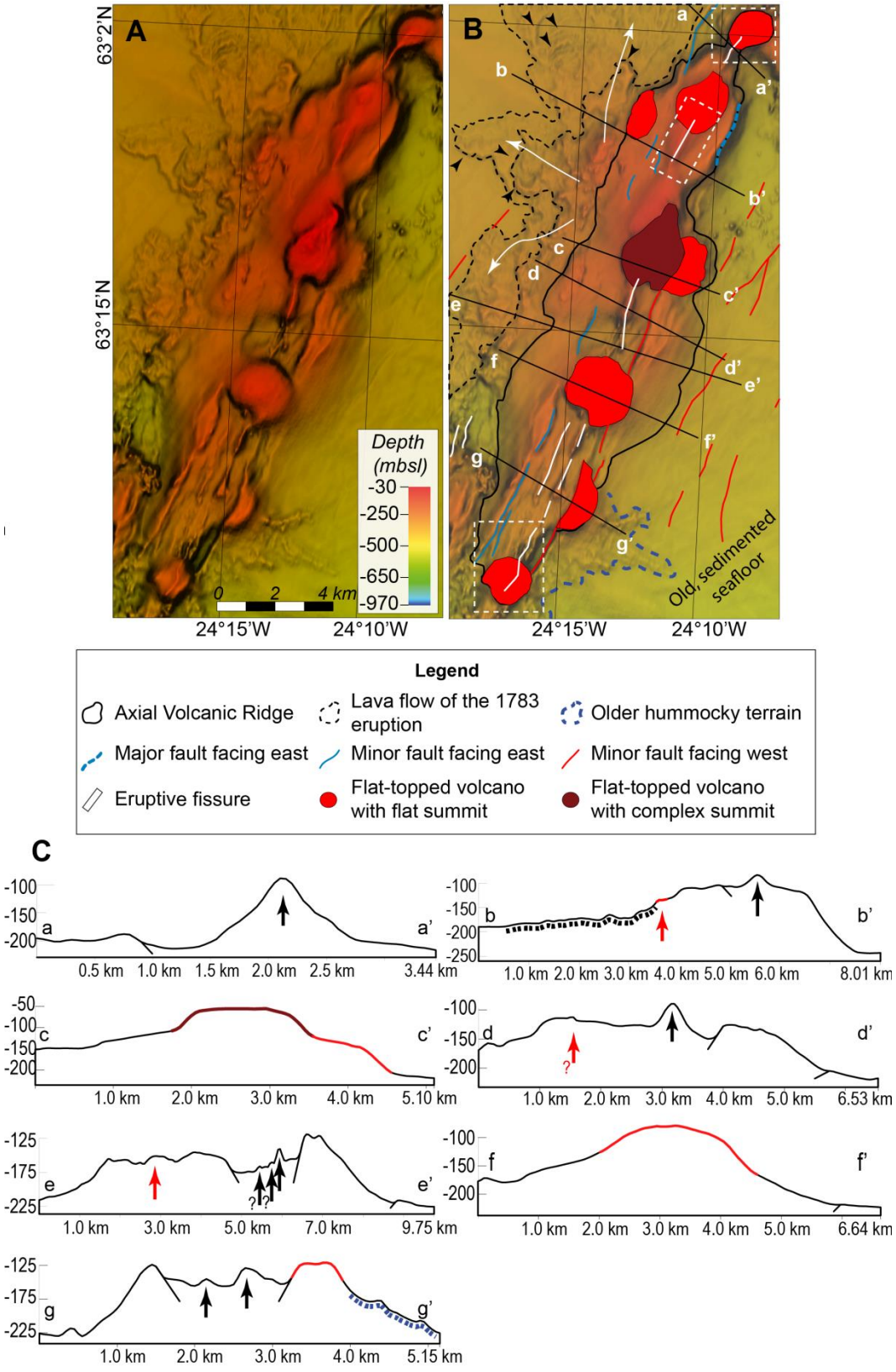

Fig. 4 Detailed interpretation of volcano-tectonic status of the AVR-1; (A) The bathymetry of the AVR. Surface of the AVR shows abnormally smooth terrain. The axis has narrow (~1.5 km wide) valley bounded by inward-facing minor faults; (B) Volcanic and tectonic features. A prominent lava flow extending outside the AVR is present in the NW region. Black arrows show lava lobes suggesting direction of the flow (marked by white arrows). An older hummocky flow (disconnected from the prominent valley) is present in the southern region but its source remains unclear. White rectangles indicate locations of younger eruptive fissures on top of flat-topped seamounts; (C) Profiles (vertical exaggeration 4x) across the AVR showing main volcanic edifices and tectonic lineaments mapped in the area.

AVR-2, similarly to AVR-1, is a subtle axial high rising above rather smooth surrounding seafloor (Fig. 5). We interpret that, based on the overall differences in terrain roughness and topographic relief between the AVR and surrounding seafloor. The seafloor around AVR is characterized by flat-topped volcanoes and hummocky terrain (slightly tectonized in SE and SW parts, Fig. 5A) while eruptive fissures are rare (Fig. 5B). The hummocky terrain surrounding the AVRs is not evidently disconnected from the AVR (unlike in the case of AVR-1) and the transition between the two is very subtle (in comparison to the sharp change seen in, e.g., AVR-3, see below). Therefore, with the resolution of our data we are unable to conclude if the hummocky terrain represents one or several generations of volcanic activity. It may suggest that the construction of AVR-2 is relatively continuous and periods of relative magmatic quiescence have not occurred. The rough hummocky terrain of AVR-2 has a high abundance of eruptive fissures (which cluster near the segment's axis) and cone/cratered volcanoes located both on and near the axis (Fig. 5B). Many of the eruptive fissures cut volcanic craters, implying that the fissures are the youngest features on AVR-2. A ring-shaped subsidence structure, ~1.5 km in diameter and ~30-40 m deeper than the surrounding seafloor, is present in the southern part of the AVR. It is cut by three segment-parallel eruptive fissures suggesting that they formed after the subsidence. Edges of this feature show slight doming, suggesting that small eruptions may have occurred along ring faults. The highest topographic feature on AVR-2 (reaching ~180 mbsl, Fig. 5A) is an eruptive fissure located just north of the subsidence structure. Its southern tip seems to also overlap the edge of the subsidence structure and, therefore, post-date it. Our interpretation suggests that present volcanic activity on AVR-2 is clustered along the axis of the segment and is concentrated in the area south of 63°05'N.

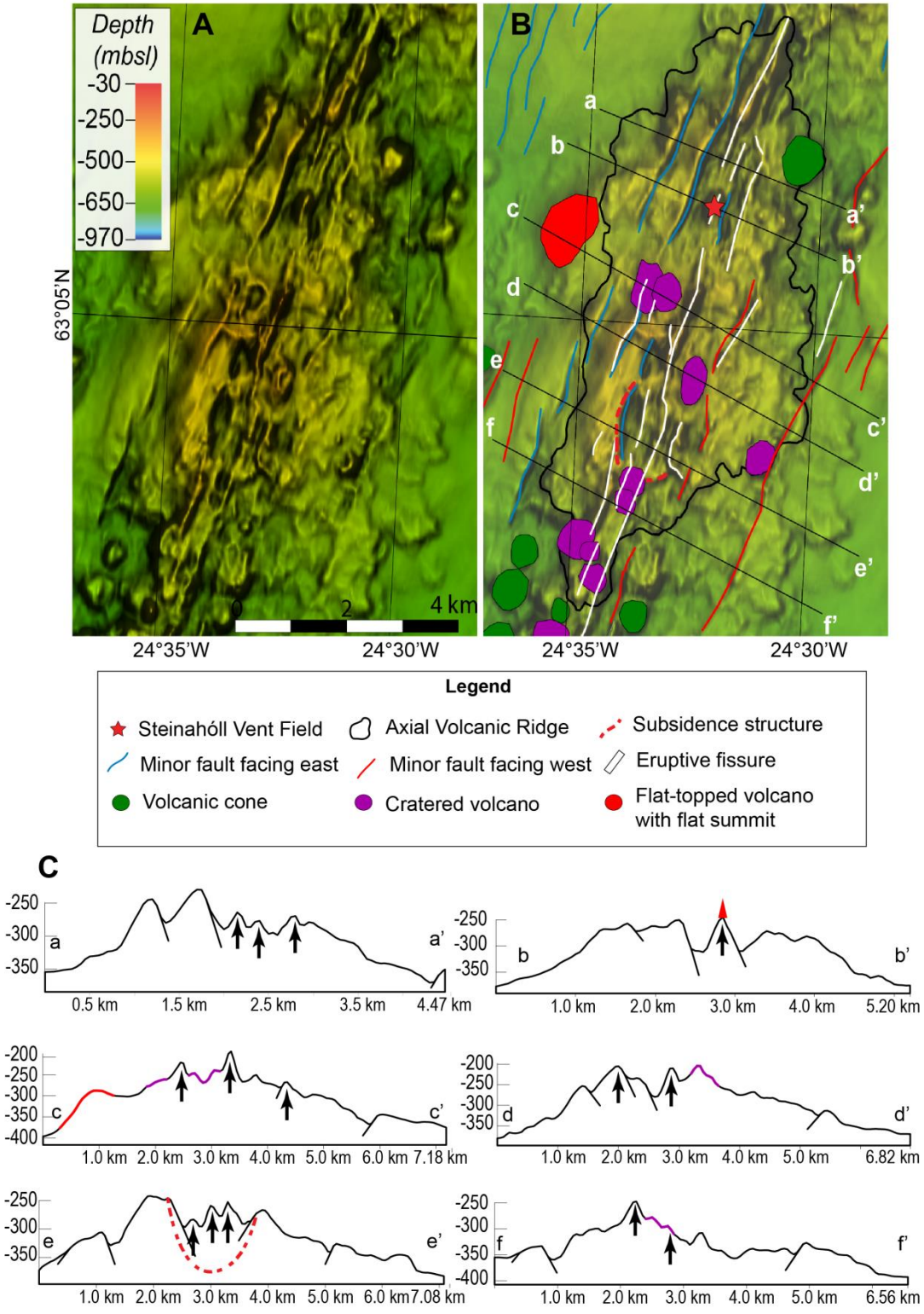

Fig. 5 Detailed interpretation of volcano-tectonic status of the AVR-2; (A) The bathymetry of the AVR. Rough hummocky terrain and cone/crater volcanoes construct both axial and near axis area, multiple eruptive fissures cluster along its axis; (B) Volcanic and tectonic features. Approximately 1.5 km in diameter subsidence structure (red dashed area) is located in the southern part of the AVR. The Steinahóll Vent Field is marked with red star; (C) Profiles (vertical exaggeration 4x) across the AVR showing main volcanic edifices and tectonic lineaments mapped in the area. Red triangle in profile ee' indicates position of the Steinahóll Vent Field.

AVR-3 (Fig. 6A) is the shortest AVR studied (see Table 1). We recognize two principle relative seafloor ages around this segment (Fig. 6B). The older AVR is characterized by eruptive fissures surmounted by cone/crater volcanoes on its western flank and by older eruptive fissures and cone/crater volcanoes with no obvious relative age relationships in the east. This older AVR has been tectonized and dismembered and is split by the currently active AVR, which appears to be constructed of volcanic cones in its outer parts but by a prominent eruptive fissure along the axis (Fig. 6A and B). This fissure cuts some of the crater volcanoes in the northern part but has one large crater volcano built on top of it in the southern region. These cross-cutting relationships suggest that the present AVR began construction from cone/crater or flat-topped volcanoes in the north followed by the formation of a long (~4 km) eruptive fissure and development of a large cratered volcano (~1.1 km in diameter). This volcano could have been constructed simultaneously with the eruptive fissure as an effect of concentration of the eruption to one vent towards the end of the eruption period (e.g., as observed during the 2014-2015 Holuhraun eruption in Iceland, Pedersen et al., 2017). It is difficult to determine whether the hummocky terrain located in the southern part of the AVR originated from the older eruptive fissure or the cratered volcano which presently sits on top of it. The northern part of the AVR-3 also shows a subsidence structure, with a sharp, south-facing and ring-shaped fault which possibly formed after the present AVR´s long eruptive fissure as we some off-set in its continuity (Fig. 6B). It appears that the present AVR is longer than the former one, as the present AVR is in direct contact with the older (smoother) seafloor at its northern and southern ends. This may indicate that presently more melt is being supplied to the segment, possibly in response to a pulse of hotter mantle material from the Icelandic hotspot (e.g., Poore et al., 2011). A higher melt supply may also be indicated by the general paucity of faulting within both the older and currently active AVR (Fig. 6A).

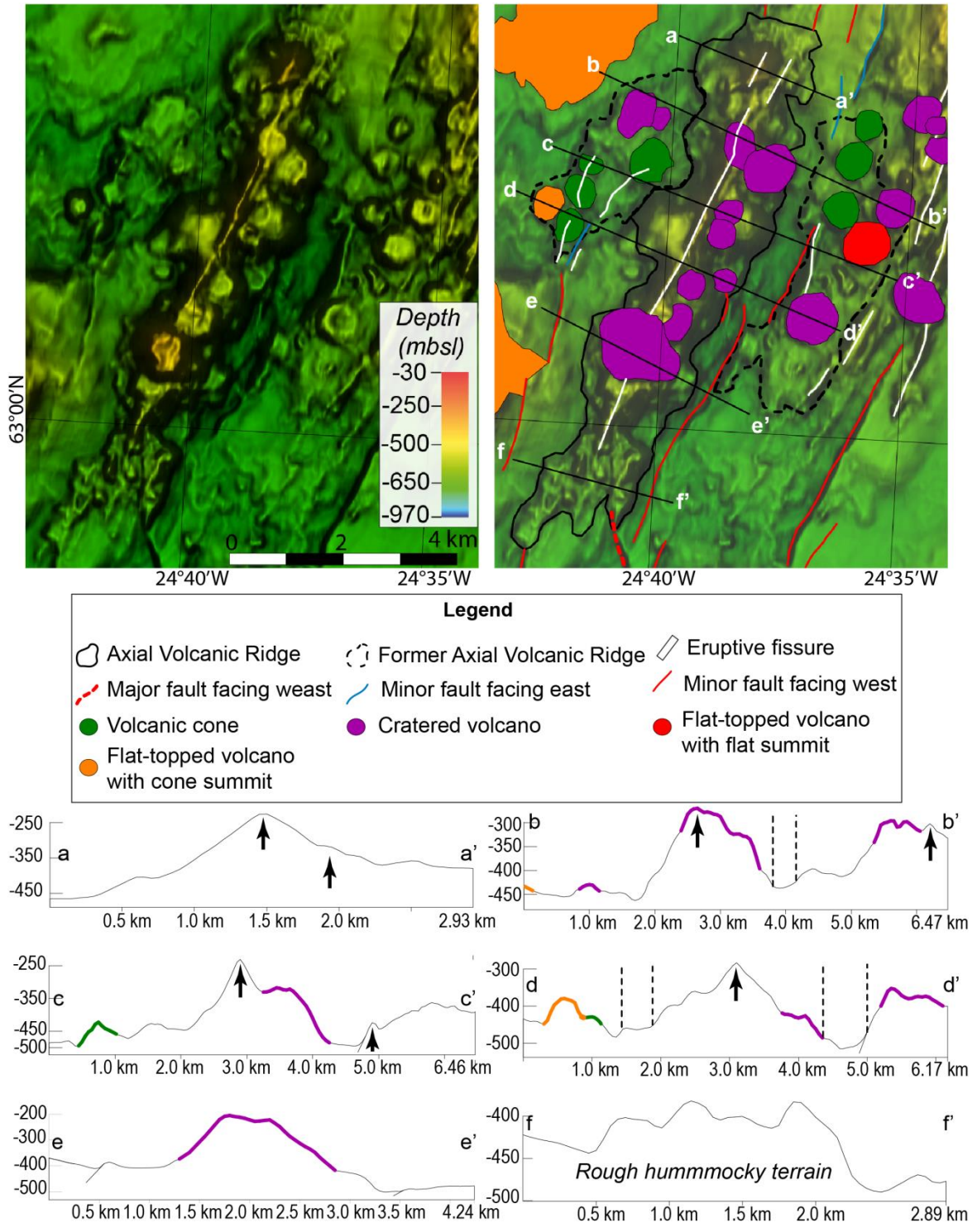

Fig. 6 Detailed interpretation of volcano-tectonic status of the AVR-3; (A) The bathymetry of the AVR. Young and rough hummocky terrain with multiple volcanic edifices is located along the segment's axis while former AVR is separated by deep basins and relatively smooth seafloor; (B) Volcanic and tectonic features. Two generations of AVR are recognized. A boundary facing SW is present in the northern part of the AVR which is probably a subsidence structure similar to one observed on AVR-2; (C) Profiles (vertical exaggeration 4x) across the AVR showing two generations of AVR, main volcanic edifices and tectonic lineaments mapped in the area.

AVR-4, unlike the three previous AVRs described, is located in a ~3.3 km wide trough (between inward-facing minor faults) rather than forming an axial high rising above the surrounding seafloor (Fig. 7A) and is the closest AVR to Iceland to be located within a

median valley. A smoother, tectonized terrain can be observed on both flanks of the AVR and outside the trough (Fig. 7B). The northern parts of this older terrain are characterized by the presence of large but tectonized flat-topped volcanoes, while only some much smaller tectonized cones can be observed in the southern regions. Large underwater flat-topped volcanoes have been proposed to form during long-lived, steady, effusive, point source eruptions on gentle slopes (Clague et al., 2000). It seems that prior to the development of AVR-4, local seafloor has been built mostly by such eruptions (Fig. 7B). However, the area located E and SE of 62°55'N and 24°45'W is characterized by a very smooth surface with some collapse structures (white-dashed rectangles in Fig. 7B). We interpret that as sheet flows and/or flattened pillow flows which erupted before the formation of AVR-4; however, higher resolution bathymetry is needed to confirm this conclusion. These observations suggest that in the past, volcanic activity around AVR-4 was mostly focused in the area north of 62°55'N with less activity in the southern region. The present AVR seems to be built by multiple, rather short (in comparison to AVR-2 or AVR-3) eruptive fissures which are sometimes observed to cut older volcanoes (Fig. 7B). Therefore, it seems that AVR-4 has experienced a transition from cone/crater-dominated volcanism followed by the development of multiple short eruptive fissures. This may reflect a reduction in effusion and eruption rates. Only three small flat-topped volcanoes appear to have formed recently on AVR-4. There is no evident change in density of volcanic features along the AVR-4 suggesting that melt is rather evenly distributed along this segment.

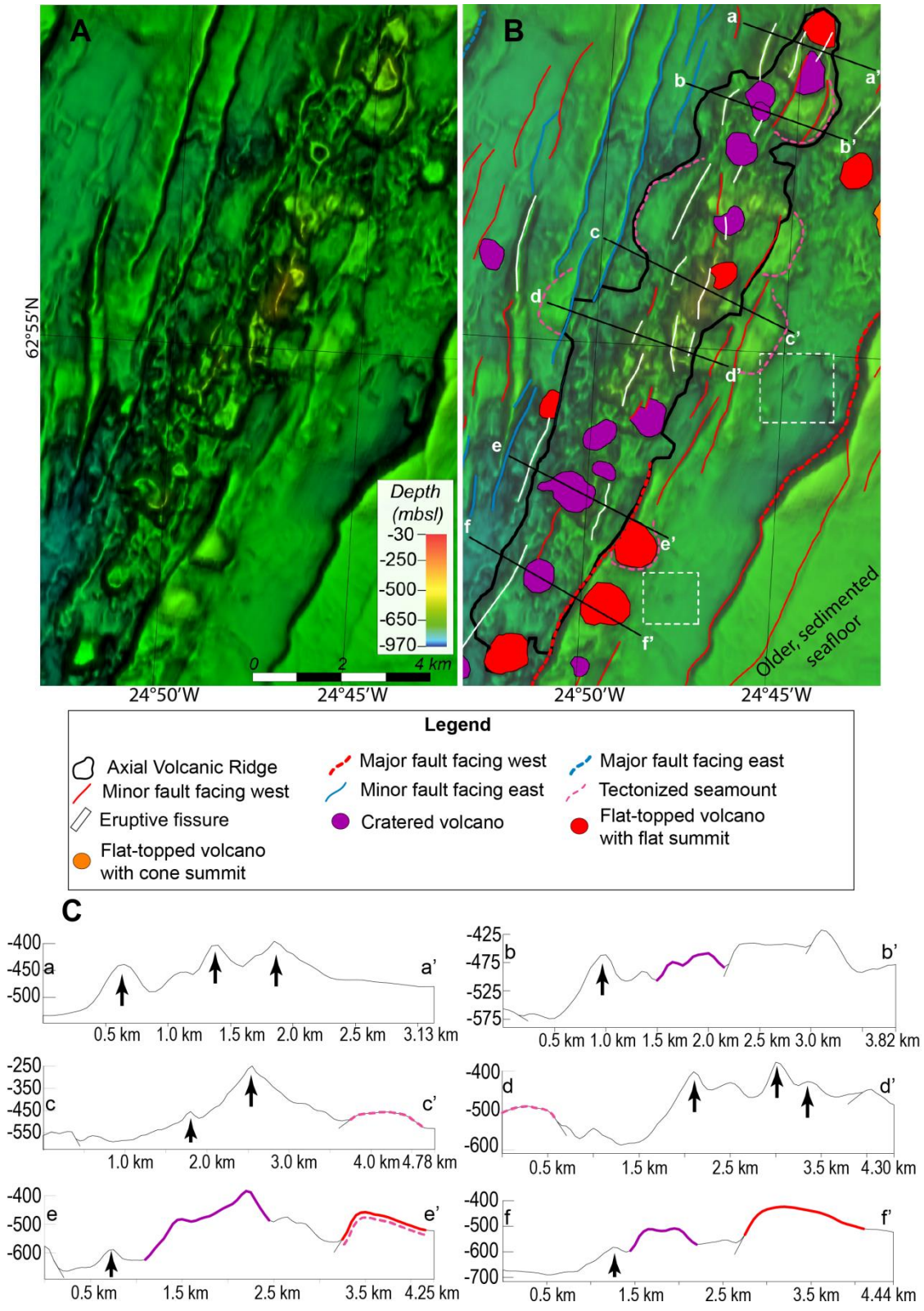

Fig. 7 Detailed interpretation of volcano-tectonic status of the AVR-4; (A) The bathymetry of the AVR. AVR-4 appears to be located in a ~3.3 km wide trough; (B) Volcanic and tectonic features. Seafloor of the flanks of the current AVR appears to be constructed by relatively large seamounts dismembered by faults due to continuous spreading, and smaller volcanic cones. An eruptive fissure overlapping older cones makes the local topographic high which reaches depth of ~250 mbsl – similar to eruptive fissure observed on AVR-2; (C) Profiles (vertical exaggeration 4x) across the AVR showing main volcanic edifices and tectonic lineaments mapped in the area.

AVR-5 is the longest (20 km) AVR in the studied area (Fig. 8). Its structure is complex, and multiple overlapping relations between volcanic features can be observed. The seafloor around AVR-5 shows no clear evidence of former AVR within the median valley. In the past (before the development of AVR-5), volcanic activity in this region was dominated by longer-lived, steady-state, volcanism, most likely sourced from the segment center; hence, at least three generations of a large, presently tectonically dismembered axial volcano can be traced W of the present AVR (Fig. 8A). Based on spreading ages, this early focusing of volcanism could have lasted for a minimum of 25 000 years before the present AVR activity developed. The flanks of AVR-5 are composed of hummocky terrain with some cone/crater/flat-topped volcanoes and rare eruptive fissures. The remains of one large cratered volcano (centered at 62°48'N and 24°58'W, white-dashed rectangle *III* in Fig. 8B), which has been partially covered by younger hummocks, can be observed on the eastern side of the segment. Significantly more circular volcanoes are present towards the AVR's axis, indicating that, with time, point-source eruptions became predominant in constructing this AVR. An alignment of smaller hummocky and bigger cratered/flat-topped volcanoes can be observed on the eastern side of AVR-5 (white-dashed rectangle *II* in Fig. 8B). Similar alignments have been recognized, for example, on the MAR near 29°N (Head et al., 1996) or the Gorda Ridge (Yeo et al., 2013), where they were interpreted as surface expressions of the underlying dikes. It seems that the size of these edifices becomes bigger towards the center of the alignment. This may indicate that at the beginning, this alignment was built by eruptions evenly distributed along a fissure but gradual cooling of the magma at both ends led to focusing of flow in several discrete locations in the central part. Hence, larger edifices have been constructed over time. A large cratered volcano (~3.5 km in diameter) showing a deep and irregularly-shaped crater marks the northern end of the AVR. Its present surface is rather smooth, indicating that it might have been inactive for a considerable amount of time and so become progressively covered by sediment. An eruptive fissure cuts the surface of this volcano just E of the crater. This fissure may be the first indication of a shift in the volcanic style in this area but further investigations are needed to correlate its age with the rest of the AVR (Fig. 8B). The southern part of AVR-5 has abundant smaller volcanic cones suggesting many point-source eruption sites, none of which reached the size of the northern cratered volcano. The axial part of AVR-5 has rough hummocky terrain, volcanic cones/craters and flat-topped volcanoes distributed towards its margins along its entire length. In the central part, hummocky terrain seems to be overlapped by a flat-topped volcano with a small conical summit. This volcano is then cut by eruptive fissures (white-dashed rectangle *I* in Fig. 8B).

This cross-cutting of the features indicates that AVR-5 was built up by multiple eruptions and shows that the eruptive fissures were the most recent. We observe a similar situation in other parts of this segment. The complex make-up of the seafloor on AVR-5 allows us to propose an evolution from early focused magmatism at a large volcanic center (W flank of the current AVR) to the development of a 20-km-long AVR which split this volcanic center. The AVR was initially more active at its central and northern parts, where it developed large circular seamounts. At present, volcanic activity seems to be migrating towards the center of the segment where the youngest eruptive fissures occur.

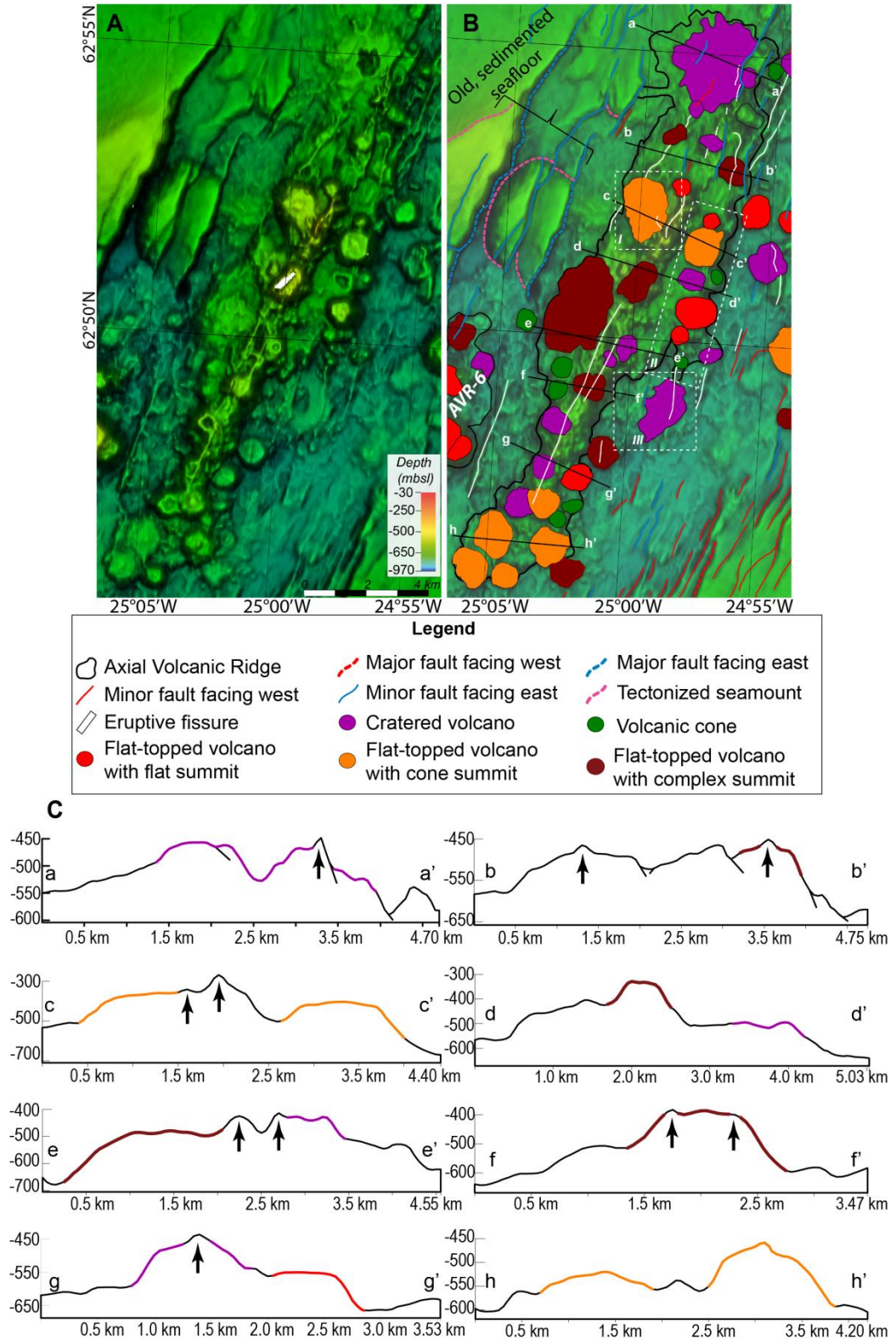

Fig. 8 Detailed interpretation of volcano-tectonic status of the AVR-5; (A) The bathymetry of the AVR. The white area on the 25°W is a gap in bathymetric data = no data; (B) Volcanic and tectonic features. Large tectonized seamount can be traced on the W side of the AVR (black bracket). White-dashed rectangles point areas of cross-correlations discussed further in the main text. Superposition of volcanic features suggests that the AVR-5 developed in multiple eruptions of which eruptive fissures were the youngest; (C) Profiles (vertical exaggeration 4x) across the AVR showing main volcanic edifices and tectonic lineaments mapped in the area.

AVR-6 is located in a ~10 km wide trough between two inward-facing major faults (Fig. 9). Outside the AVR, in the central part of this segment, a large (~7.5 km wide), relatively smooth yet visibly tectonized axial volcano can be traced for ~3 km to the W and E of the present neovolcanic zone, suggesting it may have begun construction ~30 000 years ago. Remains of the volcano are visible even outside the axial trough, implying that focused point-source volcanism was present here even before the trough developed. Large central volcanoes like this require localized eruptions of large volumes of lava (often as sheet flows) over a protracted time period, are usually underlain by thickened crust and often have axial magma chambers (AMC) associated with them (Cannat et al., 1999a; Cannat et al., 1999b; Escartin et al., 2001; Sauter and Cannat, 2010; Escartín et al., 2014). In more recent times, a ~1.5 km wide graben with hummocky terrain, eruptive fissures and volcanic cones has developed through the central part of this old seamount (Fig. 9A). Observations from the Lucky Strike central volcano (37°15'N, MAR) suggest that such structures develop in times of decreased melt supply to the segment (Escartín et al., 2014). Past volcanic output at Lucky Strike was sufficient to cover any tectonic features (faults/fractures) associated with spreading but presently the neovolcanic zone is confined to a narrow graben located at the volcano's summit. The former axial volcano on AVR-6 shows some tectonic deformation, suggesting that volcanic output here was not sufficient to cover all faults/fractures, unlike at Lucky Strike. In the southern part, AVR-6 has rough (yet tectonized) hummocky terrain with some coned/cratered volcanoes and very few eruptive fissures. In the central part a larger volcanic cone and more eruptive fissures can be distinguished. Towards the north, the highest density of eruptive fissures is seen, although coned/cratered and flat-topped volcanoes become the most numerous features (Fig. 9B). This may indicate that, presently, volcanism on AVR-6 is migrating northwards where lower effusion rate eruptive fissures are being fed by laterally propagating dikes (originating from short-lived magma reservoirs) while circular edifices have higher effusion rates and may have more established magma reservoirs. Numerous circular volcanoes and smooth seafloor can be observed outside the AVR (both on E and W side) but we are unable to conclude if they belong to a former AVR (Fig. 9B). Nevertheless, their presence implies that in the past more voluminous, point-source eruptions constructed the surrounding seafloor. The smooth seafloor observed SE of the AVR-6 probably represents old and slightly sedimented sheet-, hummocky or lobate flows, as Ruddiman (1972) and later Litvin (1984) suggested that sediments (whose accumulation could significantly smooth the seafloor) do not accumulate along the axis of the Reykjanes Ridge but rather get swept away and deposited on the ridge flanks. Therefore, sediment accumulation cannot solely be

responsible for the observed seafloor smoothness. Nevertheless, the age and source of these lava flows remains unknown.

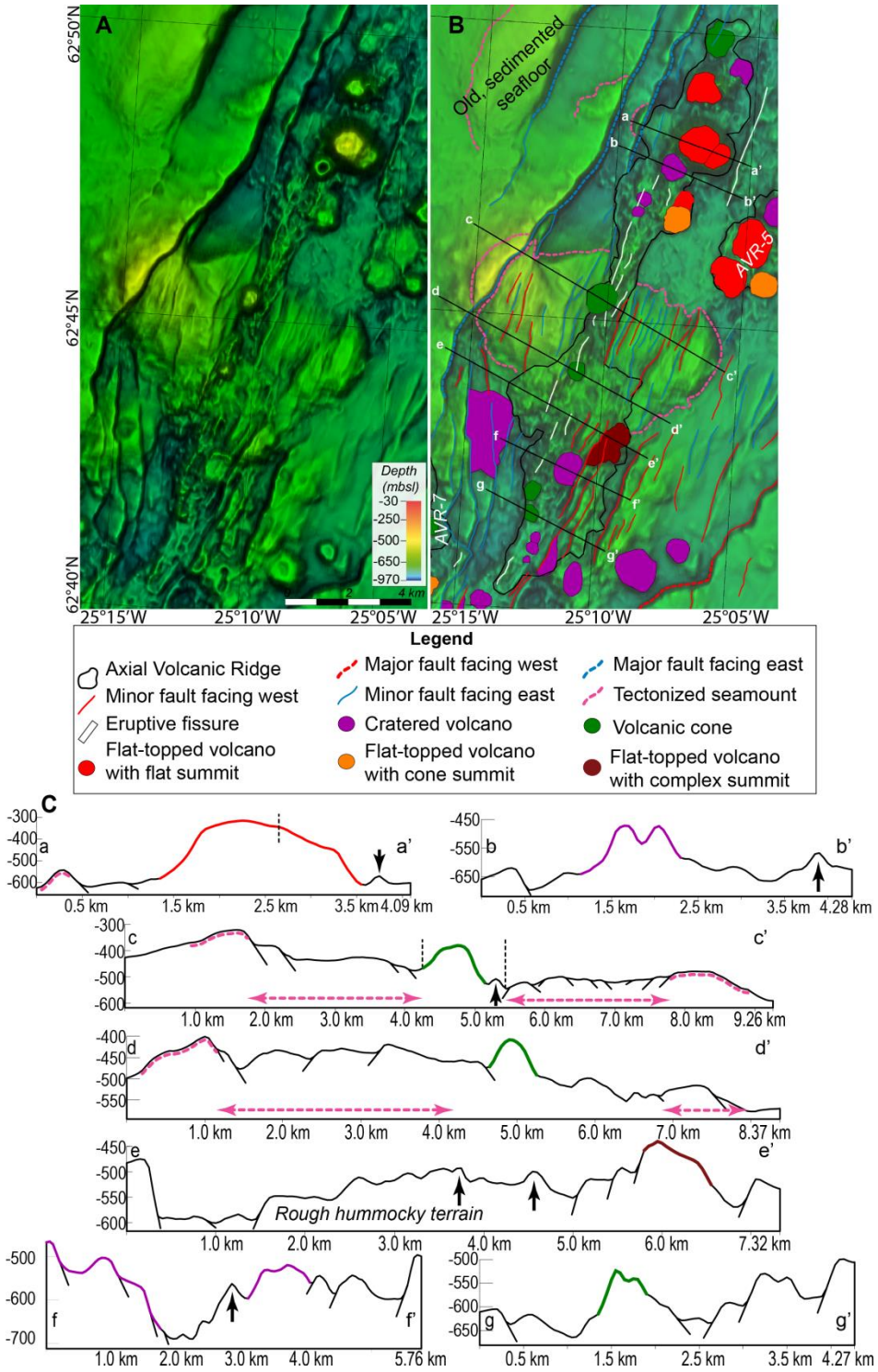

Fig. 9 Detailed interpretation of volcano-tectonic status of the AVR-6; (A) The bathymetry of the AVR; (B) Volcanic and tectonic features. A large (~7.5 km in diameter) and tectonically deformed axial seamount can be observed. The neovolcanic zone around AVR-6 is narrow reaching ~11 km. The area around AVR-6 is smooth and probably covered by sedimented lava flows which source remains unknown; (C) Profiles (vertical exaggeration 4x) across the AVR showing main volcanic edifices and tectonic lineaments mapped in the area.

AVR-7 is comparable in length, width and surface morphology to AVR-3 (Fig. 10). The bathymetric coverage around this region is limited but it appears that AVR-7 is, as with AVR-5 and -6, an axial high located within a median valley. The surrounding seafloor is rougher in comparison to neighboring AVR-6, with one tectonized cratered volcano located between the two (white-dashed box *II* in Fig. 10B). The western flank of the AVR has an old eruptive fissure overlapped by a flat-topped volcano, which has a smaller cone on top (white-dashed box *I* in Fig. 10B, 62°40'39.63"N; 25°20'17.05"W). The eastern flank shows older tectonized volcanic cones and some volcanic craters (white-dashed rectangle *III* in Fig. 10B). Both of these features are separated from the current AVR by deeper basins (similar to AVR-3); hence, they probably belong to a former AVR which got split and dismembered by ongoing spreading. The alignment of features on the western flank of AVR-7 (box *I* in Fig. 10B) resembles those observed on the eastern flanks of AVR-3 and -5, and may indicate an underlying dike. The location of flat-topped volcanoes in the southern part of the former AVR suggests that volcanic activity migrated southwards in the past where point-source eruptions constructed early AVR-7 (Fig. 10B). The most recent accretion is dominated by magmatic processes, as the AVR shows very few tectonic lineaments. The outer parts of the current AVR are constructed by coned/cratered volcanoes but a prominent eruptive fissure cutting older cones is present along the AVR's axis, north of 62°40'N (Fig. 10B). A large (~1.8 km in diameter) flat-topped volcano with a noticeable small cone at the summit (centered at 62°39'N and 25°21'W) is present at the SW extension of the eruptive fissure of the former AVR and overlaps some cratered/coned edifices and eruptive fissures of the present AVR-7. This indicates that it is the youngest (latest formed) volcanic feature in the area. A small cone at its summit suggests single vent eruptions. Large flat-topped volcanoes (e.g., along Kolbeinsey Ridge) show surface roughness similar to that observed here at comparable bathymetric resolution. They are mostly built by high effusion rate sheet flows (Escartín et al., 2014; Yeo et al., 2016); therefore, we suggests that the flat surface of the big volcano on this AVR may represent such sheet flows. The position of this volcano may imply that volcanism has migrated even further south from the older eruptive fissure (southern part of the white-dashed rectangle *I* in Fig. 10B). A magma reservoir probably developed under this volcano and continuous melt supply then led to construction of this large edifice. Unfortunately, with our data we are unable to conclude whether the flat-topped volcano and young eruptive fissure stretched along the AVR's axis are of the same or similar age. However, because both these features appear to be younger than other parts of the AVR, it seems that the two eruption mechanisms (one constructing a flat-topped volcano and the other constructing

hummocky terrain) can coexist and simultaneously erupt on one AVR at approximately the same time. A similar situation has been observed on an AVR located at 45°N on the MAR (Yeo and Searle, 2013).

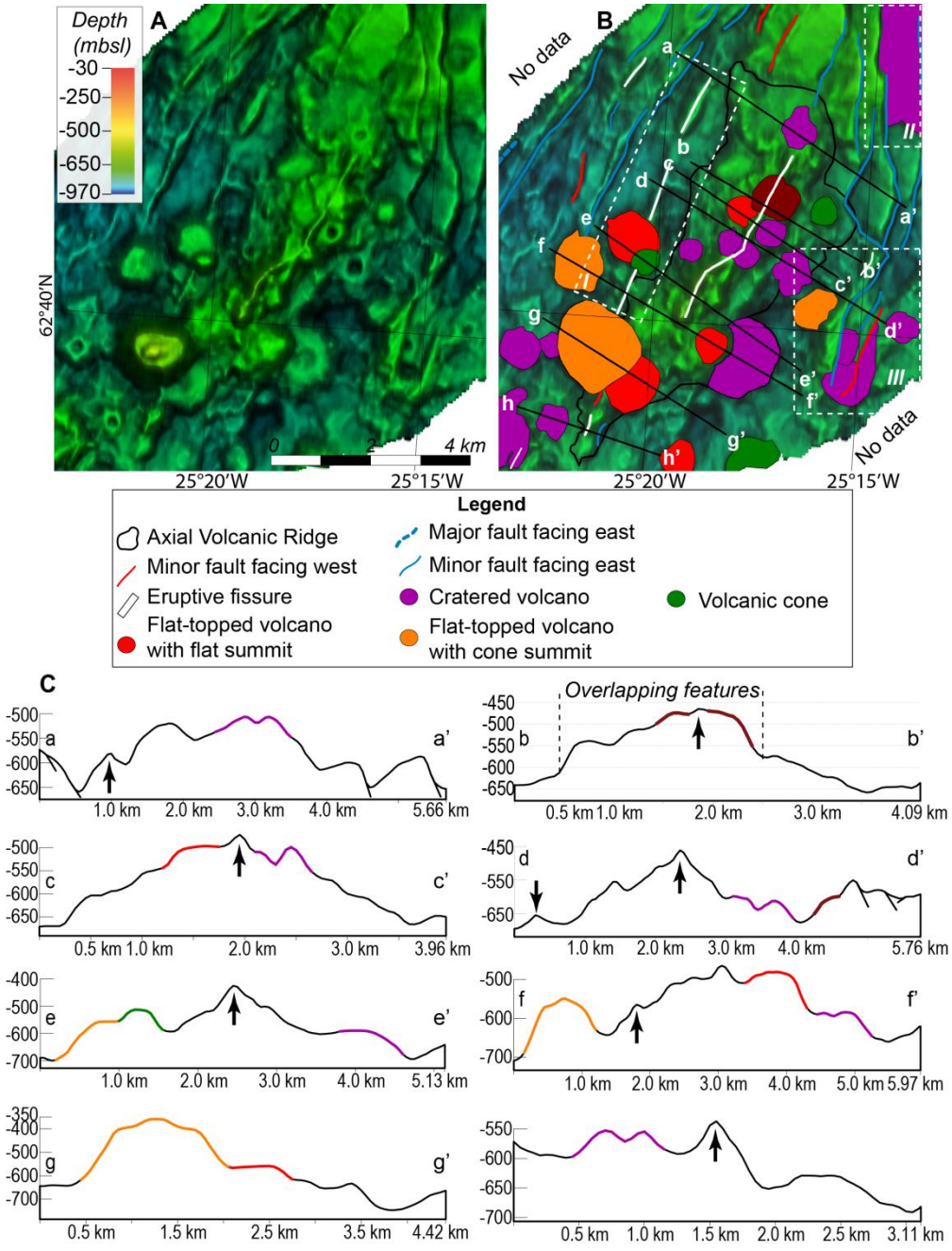

Fig. 10 Detailed interpretation of volcano-tectonic status of the AVR-7; (A) The bathymetry of the AVR; (B) The volcanic and tectonic features. Remains of a former AVR can be observed on the western and eastern flanks of the present AVR. White-dashed rectangles point areas of cross-correlations discussed further in the main text. Cross-correlations and superposition of observed flat-top and the eruptive fissure suggests that two eruption mechanisms may co-exist on AVR-7; (C) Profiles (vertical exaggeration 4x) across the AVR showing main volcanic edifices and tectonic lineaments mapped in the area.

5 Discussion

5.1 Volcanism on Axial Volcanic Ridges

Our interpretations (summarized in Tab. 1) based on the new bathymetric data show that the 4-stage evolution model for AVRs (fissure → conical volcano → shield volcano → tectonic dismemberment) proposed by Murton and Parson (1993) and Parson et al. (1993) does not reflect the construction and status of volcanic activity of the AVRs studied here. If their model was accurate we would expect a given AVR to show characteristic of only one evolutionary stage. Conversely, with our higher resolution bathymetric data we can conclude that this is not the case. Like them, we believe the surface morphology is closely linked to the presence or absence of melt in the subsurface; however, our observations suggest a much more complex magma delivery system than the periodic arrival of large melt batches to the entire segment which they proposed. Instead we propose that the surface morphologies observed here are more likely to reflect the presence of multiple small magma reservoirs (e.g., Sinha et al. (1998) imaged small magma lens beneath an AVR near 57°N on the southern RR) and that the spatial distribution and temporal variability of magma supply will control the style and location of volcanism on any one segment. This has been suggested for AVRs elsewhere on the Mid-Atlantic Ridge, e.g., near 45°N (Yeo, 2012), where it has been shown that one end of an AVR experienced robust volcanism (primarily magmatic extension) while the other end underwent tectonic deformation (primarily tectonic extension). These observations suggest that melt does not need to be equally available along the entire length of a segment and one AVR may display volcanic activity in multiple locations (e.g., not only at an AVR crest), at different times and by different eruption mechanisms. It appears that along some segments (AVR-3 and AVR-7) the availability of melt has not changed significantly over time, as the geometry of currently active AVRs follows the patterns of former AVRs. Using our data we were unable to confidently recognize former AVRs in the case of the remaining five AVRs. It is possible that the boundaries between former and current AVRs are very subtle or that these former AVRs have been strongly eroded by tectonic deformation, and/or covered by sediments. The AVR-3, southern part of AVR-5, northern part of AVR-6 and AVR-7 show robust volcanic activity and at the same time appear hardly dissected by faults suggesting that they are currently undergoing primarily magmatic extension - especially the region of southern AVR-5 and northern AVR-6 is the locus of the most robust volcanism on the RR between 62°39'N and 63°30'N. These AVRs have high numbers of seamounts, with AVR-5 showing the highest abundance (6 per 10 km^2). At the same time, AVR-3 and AVR-5 show the lowest fault density of 59 m km^2 and 60 m km^2, respectively (see Table 2).

On the other hand, AVR-1, AVR-2, AVR-4 and the southern part of AVR-6 seem to be presently melt-starved as they display much stronger tectonic deformation or are developing in a narrow trough (which has been suggested as an indication of melt starvation, e.g., at the Lucky Strike (Escartín et al., 2014)). These AVRs show lower number of seamounts (1 per 10 km^2 on AVR-1) and high fault density (100 m km^2 and 116 m km^2, on AVR-1 and AVR-6, respectively). Volcanism is not solely confined to the crest of the studied AVRs but may also occur across the entire width of an AVR, building, for example, young eruptive fissures or young volcanic cones on the margins of AVRs (e.g., AVR-2, AVR-3 and AVR-7). In some cases volcanic activity seems to be migrating along the segments; hence, on some AVRs robust volcanism is focused in central parts while in other cases it is concentrated at the segments ends. Based on the observations along the southern RR, Sinha et al. (1998) suggested that variations in the availability of highly permeable conduits through the lithospheric uppermost mantle controls generation and migration of melt along the ridge axis. If batches of melt constructing AVRs are small and transient, we would not expect them to migrate over long distances along the segments as they would probably solidify fairly quickly, e.g., due to hydrothermal cooling. Therefore, it appears that these melt batches are rather localized and small areas of the segments are affected. It seems possible that magma may be laterally transported from such magma reservoirs (as, for example, observed during the recent Holuhraun eruption in 2014-2015, Sigmundsson et al., 2014); yet it is still likely that such transport does not extend away from a given AVR. Our observations also suggests that melt supply to the segments is time-dependent, although with our data set we are unable to put further constrains on the time span involved. We did not observe an increase in volcanic activity with increasing latitude (towards Iceland) suggesting that there is no connectivity in melt supply between the AVRs.

Table 2 Main statistics of faults mapped on and around individual Axial Volcanic Ridges.

No.	Cumulative fault length (km)	Average fault length (km)	SD	Fault density (m km^2)
AVR-1	194	2.46	1.98	100
AVR-2	140	1.72	1.35	78
AVR-3	111	2.41	2.60	59
AVR-4	187	2.49	3.00	83
AVR-5	134	2.06	2.47	60
AVR-6	207	2.25	2.18	116
AVR-7	67	2.40	2.30	64*

*Minimum vale due to limited bathymetric cover around the AVR

5.2 Similarities and differences between the volcano-tectonics of Reykjanes Peninsula and Reykjanes Ridge

Recently, Pedersen and Grosse (2014) classified volcanic edifices on the RP based on their morphometry and eruption environment, and distinguished subaerial (shield) from subglacial volcanoes (glaciovolcanoes). They further extended their classification/terminology according to Russell et al. (2014), and classified the glaciovolcanoes on the RP as (1) elongated tindars, and (2) conical, complex and flat-topped tuyas. One could assume that this terminology could be further extended to the submerged RR; however, this could be an over-interpretation, as the formation mechanisms of volcanic edifices may be fundamentally different between the subglacial and seafloor environments. For instance, the significantly higher cooling rate of lavas erupted on the seafloor and the effect of depth on volatile exsolution leads to different behavior of lava (e.g., Batiza and White, 1999); hence, different morphologies and edifice may be constructed. Nevertheless, similarly to the RP, we also observe that volcanic edifices on the RR can be categorized into elongated (eruptive fissures) and circular (cone, cratered and flat-topped) edifices. On the RP, elongated tindars and eruptive fissures (crater rows) follow the overall strike of the fissure swarms, i.e., faults and fractures (Pedersen and Grosse, 2014), suggesting strong tectonic control of their formation. We observe the same pattern along the RR, where the majority of the eruptive fissures strike subparallel to faults and AVRs (Fig. 1B and Table 1). We calculated volumes of 10 eruptive fissures for which, given the resolution of our data, we could best determine their surface extent. Our volumes range from 0.0002 to 0.013 km^3 (Average=0.004 km^3, SD=0.005) which is ten times smaller than the volumes of tindars on the RP (n=13, volumes: 0.0016-0.0822 km^3; Average=0.018, SD=0.027) calculated by Pedersen and Grosse (2014). They also show that the transition between elongated and circular edifices lies in the volume range 0.01-0.1 km^3, which may suggest an evolutionary nature of eruptions from fissure to point-source eruptions (Pedersen and Grosse, 2014). Our calculations overlap with this range supporting this suggestion; however, they should be treated with caution as volumes of more recent (historic) eruptions on the RP (which constructed crater rows and not tindars) have not been included in the calculations of Pedersen and Grosse (2014). Unlike on the RP (e.g., Sæmundsson, 1979; Rossi, 1996), large shield volcanoes have not been observed on the RR. This implies that over the past ~2 Ma very long lived (nearly continuous), high effusion rate and low viscosity eruptions have not occurred in our submarine study area. Ten times greater volumes of volcanic edifices on the RP indicate that melt supply there is greater that on the RR but there are no direct estimations

of the sizes of magma reservoirs on the RP; however, submarine eruptions are expected to be less voluminous due to high confining pressure which suppresses magmatic volatile expansion, and hence, smaller volumes are erupted and smaller volcanic edifices are built.

On the RP, faults and fractures show a range of orientations in discrete structural domains in response to obliquity angle, proximity to volcanic centers and environment (magmatic vs amagmatic extension) in which they formed (Clifton and Schlische, 2003; Clifton and Kattenhorn, 2006). It has been observed that on the margins of fissure swarms, faults and fractures strike more perpendicular to the overall spreading orientation while along their axes they are more parallel to the trend of eruptive fissures (Clifton and Schlische, 2003). Given the resolution of our data, we are unable to map faults and fractures with the level of detail presented by Clifton and Schlische (2003) and Clifton and Kattenhorn (2006). Nevertheless, we observed that the faults in our study area do not cluster into structural domains (in contrast to RP) but rather strike subparallel to the individual AVRs (orientations between 18° and 29°, see Tab. 2) with the majority having orientations between 15° and 30° (Fig. 11). These orientations are orthogonal to the ~105° spreading direction suggested by DeMets et al. (1994). Similar patterns have been observed by Searle et al. (1998) on the RR south of our study area showing that the spreading direction is relatively uniform along the entire length of the RR. Murton and Parson (1993) and later Searle et al. (1998) suggested that faults orthogonal to spreading direction on the RR form in response of seafloor to plate separation induced extension which, therefore, appears to control formation of AVRs and faults also in our study area.

We have not observed along-ridge variations in either cumulative fault length or fault density on and around individual AVRs (Tab. 2); however, we noticed that faults on the AVRs are, overall, shorter, straighter and fewer in number in comparison to the AVR flanks where they are longer, more sinusoidal and more abundant (Fig. 11). Similar patterns have been observed within and around fissure swarms on the RP (Clifton and Schlische, 2003; Clifton and Kattenhorn, 2006) suggesting that also along the AVRs on the RR presence/absence of magma in the crust and point in time in the magmato-tectonic crustal extension period influences fault patterns.

The AVRs studied here show no clear pattern of eruptive fissures clustering along the segments axes and circular edifices building up on their flanks, which is in contrast to the RP (e.g., Jakobsson et al., 1978; Sæmundsson, 1979; Pedersen and Grosse, 2014). Instead, our observations show that circular edifices, e.g., cratered and flat-topped volcanoes, can also be constructed along the AVRs axes (e.g., AVR-3 and AVR-7). It implies that melt is supplied to

the AVRs over extended period of time leading to construction of larger, point-source volcanic vents. It also suggests that tectonism and stress regime within the crust of the RR is not the primary factor controlling eruption mechanisms on the RR, and we attribute this to the overall different stress regimes, e.g., lack of transform faults and non-transform offsets along the studied section of the RR.

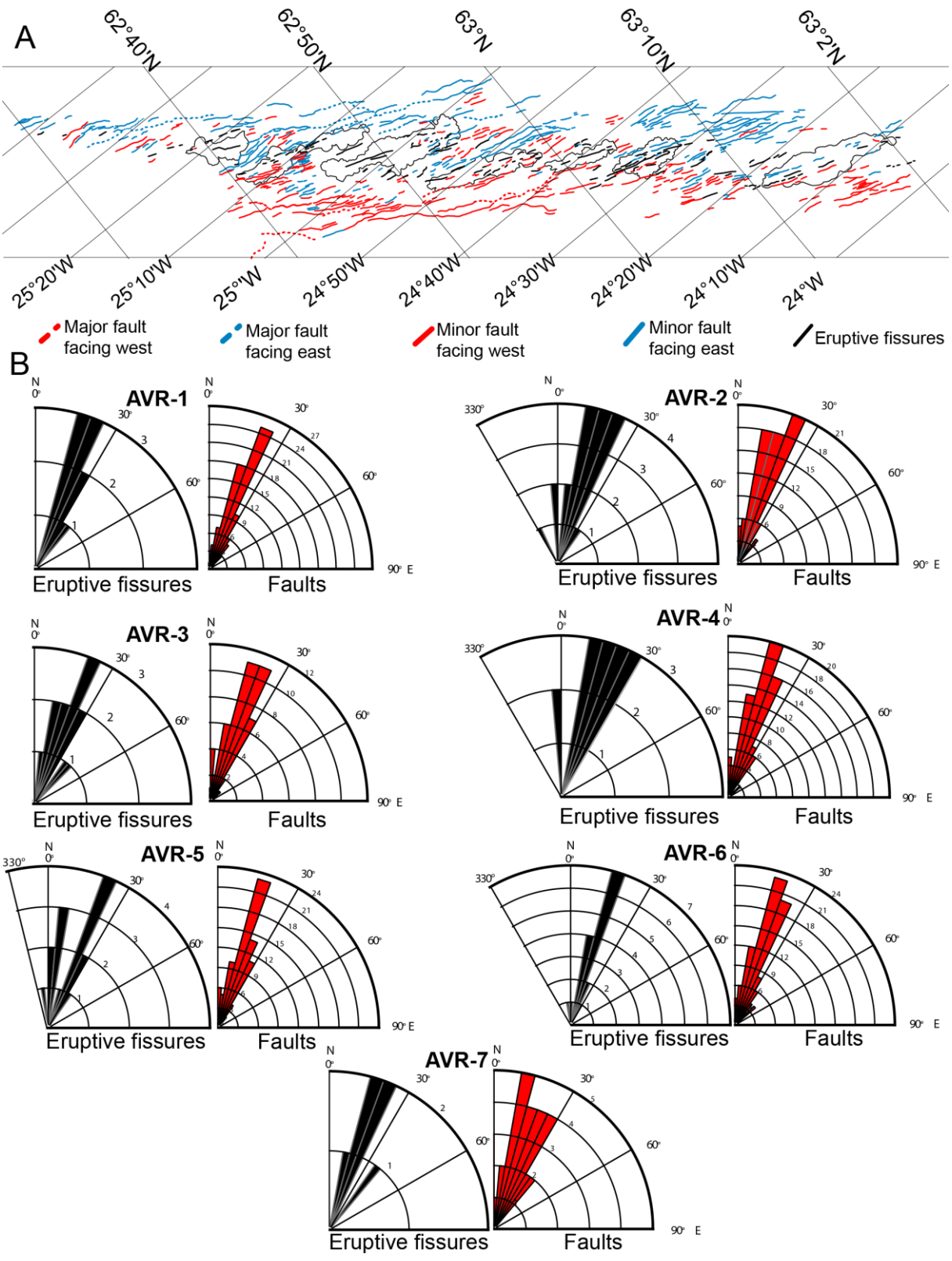

Fig. 11 (A) Faults and eruptive fissures mapped in the study area and outlines of AVRs (black thin lines); (B) Rose diagrams showing strikes of eruptive fissures and faults on and around individual AVRs.

5.3 Volcanic control of venting at Steinahóll Vent Field and elsewhere

The Steinahóll Vent Field is located in the northern part of the AVR-2 (Figs. 5B) in an area characterized by a ~500 m long eruptive fissure located between two east-facing faults,

although the site is not directly located on the scarp or extension of any fault (Fig. 5A). The area around the vent site is a rough volcanic terrain (eruptive fissures and hummocks). Our interpretation of the geological evolution of AVR-2 (see section 4.3) suggests that at least some of the eruptive fissures are the youngest features on this AVR as the post-date cratered volcanoes and observed subsidence structure (Fig. 5B). Therefore, venting at Steinahóll may be driven by the heat input from the dikes intruding at depth along this segment (some of which reach the seafloor and erupt forming eruptive fissures) while the crustal permeability is sustained by the active faults. It is possible that the Steinahóll field is cooling this entire 10.2 km long segment through a system of sub-bottom faults and fractures, as it has been shown that one black smoker can cool up to 50 km of the spreading axis (e.g., Hannington et al., 2010).

It has been suggested that the oceanic crust formed on the RR may be cooled by widespread off-axis 'diffuse' venting rather than on-axis focused high-temperature vents (German et al., 1994; Devey et al., 2010). Pałgan et al. (2016) proposed that such diffuse venting may be controlled by off-axis dike intrusions, as observed in off-axis regions of Iceland. However, evidence for such a cooling mechanism has not yet been found along the RR. While we assume the magma supply to the RP to be more robust, based on the volumes of the edifices and flows, the frequency of hydrothermal fields there far exceeds that expected for a normal spreading-ridge (German et al., 1996). The morphological similarities between the RP and the RR indicate that both the physical characteristics (types of observed volcanic edifices, orientation and geometry of faults and cross-cutting of the features) and heat source required for hydrothermal flow on the RP are present at all the AVRs studied. We would therefore expect all or most to host hydrothermal systems. Submarine hydrothermal venting naturally focuses towards topographic highs (Bani-Hassan et al., 2012; Titarenko and McCaig, 2015) or develops in regions where the most recent volcanic activity occurred and/or volcanic and/or tectonic features cross-cut (Chadwick et al., 2001). Taking this into account, Figure 12 shows areas along the RR between 62°30'N and 63°30'N where we postulate that sites of hydrothermal activity may be located.

On AVR-1, eruptive fissures are sites of the youngest volcanic activity and are probably post-glacial (younger than 12 000 years). They may host hydrothermal activity similarly to that seen at the Brennisteinsfjöll area on the RP. Despite one known hydrothermal field on the AVR-2 (northern part) it appears that young eruptive fissures may be present at its southern end as well, where they cut a ring-shaped subsidence structure. One of these fissures is the highest topographic feature on the AVR making it a preferable location for a hydrothermal

system to develop. On the AVR-3 we predict that hydrothermal activity may be located in the southern part of the segment where a relatively large cratered volcano overprints an eruptive fissure running along the AVR crest. The volcano's summit reaches depths of ~200-250 mbsl. The Steinahóll field on AVR-2 is located at a similar depth. In Iceland, high-temperature geothermal activity is sometimes associated with calderas and subsidence structures, e.g., Krafla (Arnórsson et al., 2008). Therefore, the two ring-shaped subsidence structures observed on AVR-2 and AVR-3 could be valid locations for future hydrothermal exploration. On AVR-4 and AVR-5, hydrothermalism may be associated with eruptive fissures (the youngest volcanic features of these segments), reaching depth of ~250 mbsl (again similar to Steinahóll) and ~300 mbsl, respectively. On AVR-6, volcanic activity seems to be migrating northwards, making the region north of 62°45'N a valid region for exploration. Particularly the shallow (~315 mbsl), flat-topped volcano with small summit cone near the northern end of the neovolcanic zone appears to be a strong target. Moreover, a strongly rifted and tectonized axial high on this AVR should form a site of increased crustal permeability and so also has high potential for development of a hydrothermal site such as those seen at Lucky Strike (Langmuir et al., 1997) or Menez Gwen (Fouquet et al., 1994). On AVR-7, both an eruptive fissure (cutting an older flat-topped volcano in the northern part) and a large flat-topped volcano (overlapping older eruptive fissures and volcanic cones in the southern part) are the youngest volcanic features of relatively similar age. However, the flat-topped volcano forms a local topographic high, reaching depth of ~360 mbsl, making it the preferable location for a hydrothermal system to develop.

Hydrothermal prospection on these sites will need to be adapted to the particular local conditions: the shallow setting of the whole area coupled with strong bottom currents associated with the North Atlantic Drift or Iceland-Scotland Overflow Water (Valdimarsson and Malmberg, 1999) and the general morphology of the plate boundary along the RR between ~59°N and Iceland (a prominent axial high with only a very shallow axial trough) may lead to very fast dispersal and dilution of hydrothermal plumes. We propose that a combination of survey methods (including near-bottom use of autonomous vehicles) would be necessary to study the incidence of hydrothermal activity along the Reykjanes Ridge and perhaps on other hotspot-influenced ridges.

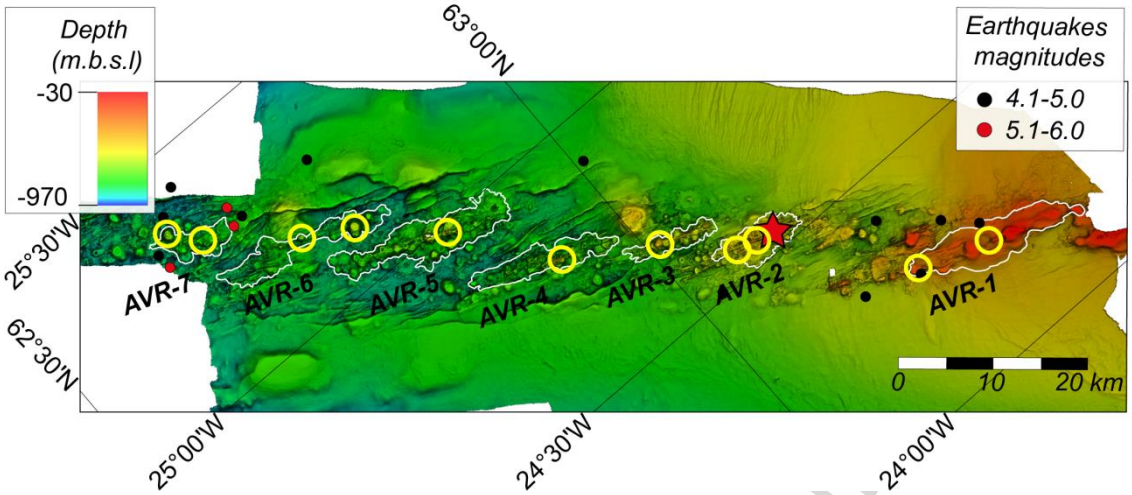

Fig. 12 Predicted locations of new hydrothermal sites along the Reykjanes Ridge between 62°30'N and 63°30'N. Seven mapped AVRs are highlighted with white outlines. Red star indicates location of Steinahóll Vent Field while red and black dots are epicenters of earthquakes from years 1950-2015 (ISC). We predict 11 new sites of hydrothermal activity based on the interpretation of Steinahóll setting, on land observations from Reykjanes Peninsula and elsewhere in Iceland. Therefore, the youngest volcanic features are expected to host hydrothermal activity. These are eruptive fissures or flat-topped/cratered volcanoes which tend to form local topographic highs. Additionally, two ring-shaped subsidence structures observed on AVR-2 and AVR-3 are also taken into consideration.

5.4 Signs of off-axis volcanism on the Reykjanes Ridge?

Although most crustal accretion occurs along the spreading axes, off- and near-axis eruptions may contribute significantly to the formation of new oceanic crust (Perfit and Chadwick, 1998). For example, fresh-looking lavas have even been sampled along the flanks of the ultraslow-spreading Southwest Indian Ridge between 9-16°E (Standish and Sims, 2010). Leroy et al. (2010) suggested that mantle plumes may cause off-axis volcanism on the flanks of slow-spreading ridges by channeling of melt along the ridge system and its distribution along the brittle-ductile boundary at depth. Off-axis eruptions may use pre-existing fractures and faults as conduits (Standish and Sims, 2010) as has also been observed on Iceland by Khodayar and Einarsson (2002) who showed examples of dikes intruded into faults on the flanks of the neovolcanic zones there.

The resolution of bathymetry presented in this paper allows us to point to a few locations along the flanks of the RR where off-axis magmatism may have occurred. Figure 13 shows three sites where hummocky volcanoes and elongated volcanic ridges striking parallel to the AVRs lie outside the ridge axis and away from the AVRs. In places, hummocky ridges rise up to 50 m above the surrounding seafloor and seem to occupy minor faults. This may indicate that, similar to ridges of different spreading rates, off-axis volcanism along slow-spreading and hotspot-influenced ridges can occur where magma uses even far off-axis faults and fractures as conduits. Off-axis volcanic edifices are known to host active hydrothermal activity and hydrothermal deposits along the flanks of East Pacific Rise (EPR) near 9°28'N

(Macdonald et al., 2002) but whether the three locations mentioned above are also hydrothermally active remains unknown. However, even if they are active they could not account for the hydrothermal sites and heat output which are missing along the RR. All three areas in Figure 13 are located near the margin of the neovolcanic terrain (e.g., Fig. 1) and ~5 km from the ridge axis. That distance is sufficient for a high-temperature system to develop away from the ridge axis as, for example, in Iceland the high-temperature site of Theistareykir (within the Northern Volcanic Zone) is located much closer to the older Plio-Pleistocene formations then the sites of Krafla and Námafjall (also within the Northern Volcanic Zone, Arnórsson et al., 2008). This implies that areas identified here are also of relevance for hydrothermal prospection. The age of these eruptions is unknown and, therefore, we cannot put further constrains on the life span of any potential hydrothermal sites. If the RR is similar to the EPR and Northern Volcanic Zone in Iceland, off-axis volcanic activity may be important for the formation of mineral deposits and the biogeography of the northern MAR.

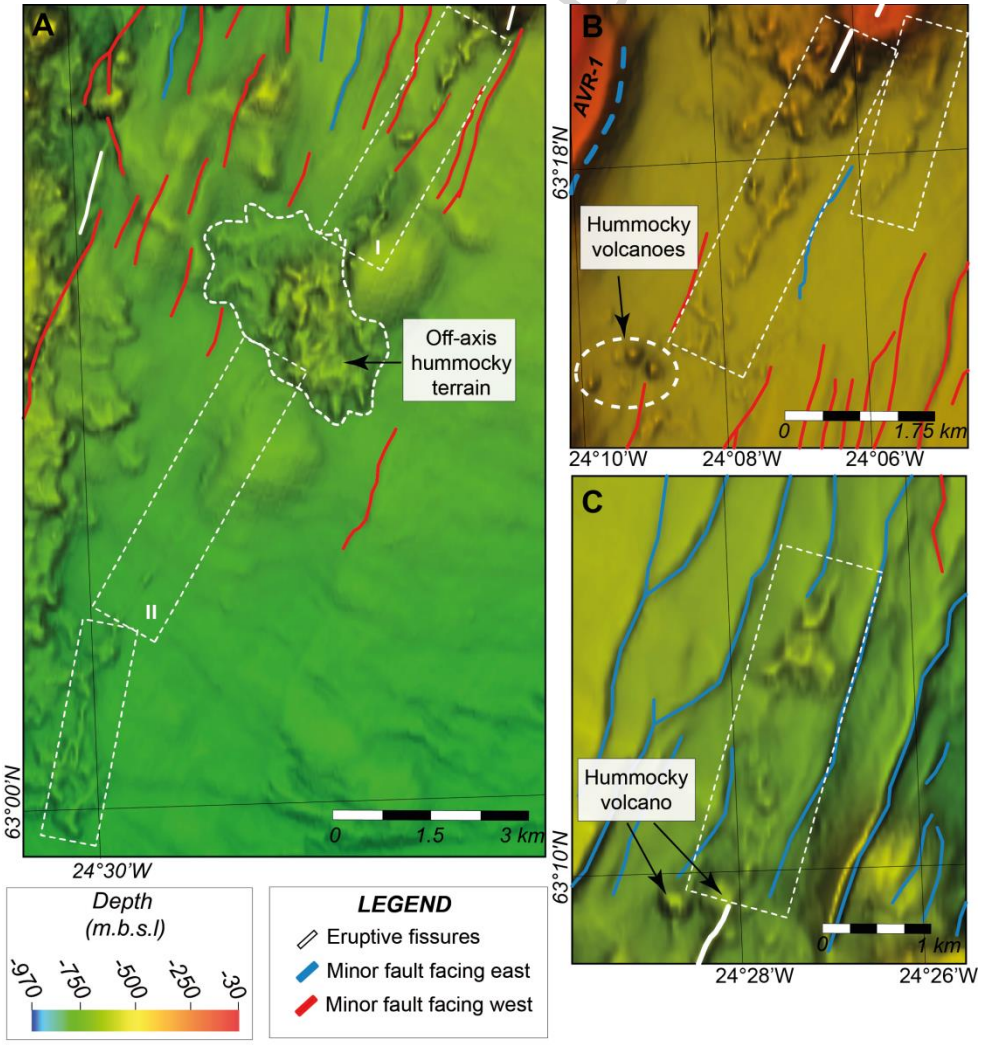

Fig. 13 Potential locations of off-axis eruption sites on the flanks of the Reykjanes Ridge between 62°30'N and 63°20'N; (A) Eastern flank of the RR with 13 km long hummocky ridge rising up to 50 m above the

surrounding seafloor. In the northern part (dashed box I) the ridge occupies west-facing fault suggesting dike injection into the pre-existing fault. In the southern are (dashed box II) hummocky ridge occupies continuation of the fault seen in dashed box I. The site is located ~5 km away from the ridge axis; (B) Eastern flank of the RR near AVR-1, where with elongated hummocky ridges strike subparallel to AVR and local faults. Few hummocky volcanoes have also been observed. Both kinds of features reach ~20 m above the surrounding seafloor; (C) Eastern flank of the RR Ridge with ~3 km long hummocky ridge which occupies east-facing fault again suggesting dike injection into pre-existing fault. Depth scale is applicable to all three panels.

6 Conclusions

The Reykjanes Ridge between 62°30'N and 63°30'N hosts seven Axial Volcanic Ridges (AVRs) which, based on their morphology and geometry, are the equivalents of the adjacent subaerial fissure swarms on the Reykjanes Peninsula, Iceland. Interpretation of the volcano-tectonic setting allowed us to identify the sites of youngest volcanic activity on each of the seven AVRs. Magma does not seem to be evenly distributed along the entire length of the AVRs, implying that formation of AVRs along the Reykjanes Ridge is more complex than the 4-stage model previously proposed. In some cases, the youngest volcanism appears to be associated with elongated eruptive fissures up to 7 km in length, suggesting strong tectonic control and low effusion-rate eruption mechanisms. In others, the latest volcanic activity seems to have a more point-source character implying longer-lived magma supply to the systems and higher effusion rates. Our interpretation suggests that Steinahóll (the only known high-temperature hydrothermal field along the ~950 km long Reykjanes Ridge) is located on top of a young eruptive fissure. This distinctive morphology strongly resembles abundant tindars (also known as hyaloclastite ridges) which are known to host geothermal activity on the Reykjanes Peninsula (e.g., Krýsuvík or near Brennisteinsfjöll). Bathymetric features similar to those observed at Steinahóll are observed on shallow regions of all the AVRs, where sometimes they are the highest topographic features. The fact that hydrothermal systems have not also been previously detected there is probably due to the sensitivity of the instruments used to search for them - topographic highs on the axial ridges of the Reykjanes Ridge are the regions where strongest currents occur, probably causing plumes to be swept away from their source and dispersed rapidly, a situation requiring near-bottom prospection, ideally with autonomous and remotely controlled vehicles. Off-axis volcanism, which on Iceland has been shown to provide permeable pathways for off-axis hydrothermal circulation, has been detected on the flanks of the Reykjanes Ridge - it remains to be seen if it is also the site of hydrothermal circulation.

Acknowledgments

We would like to thank Nico Augustin for help with the Terrain Texture Shading technique and discussions. We thank the two anonymous reviewers for their valuable comments which greatly improved this paper. Ólafur S. Ástþórsson and Guðrún Helgadóttir from the Marine Research Institute in Reykjavik are thanked for collecting and providing the bathymetric data used in this study. Financial support through the Helmholtz graduate school HOSST to D.P. (grant VH-KO-601) is gratefully acknowledged.

7 Literature

Anderson, M.O., Hannington, M.D., Haase, K., Schwarz-Schampera, U., Augustin, N., McConachy, T.F., and Allen, K., 2016, Tectonic focusing of voluminous basaltic eruptions in magma-deficient backarc rifts: Earth and Planetary Science Letters, v. 440, p. 43–55, doi: 10.1016/j.epsl.2016.02.002.

Arnórsson, S., 1995, Geothermal systems in Iceland: Structure and conceptual models—I. High-temperature areas: Geothermics, v. 24, p. 561–602, doi: 10.1016/0375-6505(95)00025-9.

Arnórsson, S., Axelsson, G., and Sæmundsson, K., 2008, Geothermal systems in Iceland: Jökull, v. 58, p. 269–302.

Augustin, N., van der Zwan, F.M., Devey, C.W., Ligi, M., Kwasnitschka, T., Feldens, P., Bantan, R. a., and Basaham, A.S., 2016, Geomorphology of the central Red Sea Rift: Determining spreading processes: Geomorphology, v. In Press, doi: 10.1016/j.geomorph.2016.08.028.

Baker, E.T., and German, C.R., 2004, On the Global Distribution of Hydrothermal Vent Fields, in German, C.R., Lin, J., and Parson, L.M., [Eds.], Mid-Ocean Ridges, American Geophysical Union, p. 245–266.

Bani-Hassan, N., Iyer, K., Rüpke, L.H., and Borgia, A., 2012, Controls of bathymetric relief on hydrothermal fluid flow at mid-ocean ridges: Geochemistry, Geophysics, Geosystems, v. 13, p. Q05002, doi: 10.1029/2012GC004041.

Batiza, R., and White, J.D.L., 1999, Submarine lavas and hyaloclastite, *in* Sigurdsson, H., [Ed.], Encyclopedia of volcanoes, Academic Press, p. 361–481.

Beaulieu, S.E., Baker, E.T., and German, C.R., 2015, Where are the undiscovered hydrothermal vents on oceanic spreading ridges?: Deep-Sea Research Part II, v. 121, p. 202–212, doi: 10.1016/j.dsr2.2015.05.001.

Brown, L., 2010, A new Technique for depicting terrain relief, NACIS Annual Meeting, Petersburg.

Cannat, M., Briais, A., Deplus, C., Escartı, J., Georgen, J., Lin, J., Mercouriev, S., Meyzen, C., Muller, M., Pouliquen, G., and Rabain, A., 1999a, Mid-Atlantic Ridge - Azores hotspot interactions: along-axis migration of a hotspot-derived event of enhanced magmatism 10 to 4 Ma ago: Earth and Planetary Science Letters, v. 173, p. 257–269, doi: 10.1016/S0012-821X(99)00234-4.

Cannat, M., Rommevaux-Jestin, C., Sauter, D., Deplus, C., and Mendel, V., 1999b, Formation of the axial relief at the very slow spreading Southwest Indian Ridge (49° to 69°E): Journal of Geophysical Research: Solid Earth, v. 104, p. 22825–22843, doi: 10.1029/1999JB900195.

Chadwick, Jr., W.W., Scheirer, D.S., Embley, R.W., and Johnson, H.P., 2001, High-resolution bathymetric surveys using scanning sonars: Lava flow morphology , hydrothermal vents, and geologic structure at recent eruption sites on the Juan de Fuca Ridge: Journal of Geophysical Research Solid Earth, v. 106, p. 16075–16099, doi: 10.1029/2001JB000297.

Clague, D.A., Moore, J.G., and Reynolds, J.R., 2000, Formation of submarine flat-topped volcanic cones in Hawai'i: Bulletin of Volcanology, v. 62, p. 214–233, doi: 10.1007/s004450000088.

Clifton, A.E., and Kattenhorn, S.A., 2006, Structural architecture of a highly oblique divergent plate boundary segment: Tectonophysics, v. 419, p. 27–40, doi: 10.1016/j.tecto.2006.03.016.

Clifton, A.E., and Schlische, R.W., 2003, Fracture populations on the Reykjanes Peninsula , Iceland: Comparison with experimental clay models of oblique rifting: Journal of Geophysical Research, v. 108, p. 2074, doi: 10.1029/2001JB000635.

Clifton, A.E., Sigmundsson, F., Feigl, K.L., Gudmundsson, G., and Arnadottir, T., 2002, Surface effects of faulting and deformation resulting from magma accumulation at the Hengill triple junction, SW Iceland, 1994-1998: Journal of Volcanology and Geothermal Research, v. 115, p. 233–255, doi: 10.1016/S0377-0273(01)00319-5.

Crane, K., Johnson, L., Appelgate, B., Nishimura, C., Buck, R., Jones, C., Vogt, P., and Rubin, K., 1997, Volcanic and Seismic Swarm Events on the Reykjanes Ridge and Their Similarities to Events on Iceland: Results of a Rapid Response Mission: Marine Geophysical Researches, v. 19, p. 319–338, doi: 10.1023/A:1004298425881.

DeMets, C., Gordon, R.G., Argus, D.F., and Stein, S., 1994, Effect of recent revisions to the geomagnetic reversal time scales on estimates of current plate motions: Geophysical Research Letters, v. 21, p. 2191–2194, doi: 10.1029/94GL02118.

Devey, C.W., German, C.R., Haase, K.M., Lackschewitz, K.S., and Melchert, B., 2010, The relationships between volcanism , tectonism , and hydrothermal activity on the southern equatorial Mid-Atlantic Ridge, *in* Rona, P., Devey, C. W., Dyment, J., and Murton, B., [Eds.], Diversity of hydrotehrmal systems on slow spreading ocean ridges, American Geophysical Union, Washington D.C., p. 133–152, doi: 10.1029/GM188.

Egloff, J., and Johnson, G.L., 1979, Erosional and depositional structures of the southwest Iceland insular margin: thirteen geophysical profiles, *in* Watkins, J.S., Montadert, L., and Dickerson, P.W., [Eds.], Geological and Geophysical Investigations of Continental Margins, Tulsa, Oklahoma, p. 43–63.

Engdahl, E.R., Hilst, R. Van Der, and Buland, R., 1998, Global Teleseismic Earthquake Relocation with Improved Travel Times and Procedures for Depth Determination: Bulletin of the Seismological Society of America, v. 88, p. 722–743.

Escartín, J., Cannat, M., Pouliquen, G., Rabain, A., and Lin, J., 2001, Crustal thickness of V-shaped ridges south of the Azores; interaction ofthe Mid-Atlantic Ridge (36°-39°N) and the Azores hot spot: Journal of Geophysical Research, v. 106, p. 21719–21735, doi: 10.1029/2001JB000224.

Escartín, J., Soule, S.A., Cannat, M., Fornari, D.J., Düşünür, D., and Garcia, R., 2014, Lucky Strike seamount: Implications for the emplacement and rifting of segment-centered volcanoes at slow spreading mid-ocean ridges: Geochemistry, Geophysics, Geosystems, v. 15, p. 4157–4179, doi: 10.1002/2014GC005477.

Fouquet, Y., Charlou, J.-L., Costa, I., Donva, J.P., Radford-Knoery, J., Pelle, H., Ondreas, H., Lourenço, N., Segonza, M., and Kingston Tivey, M., 1994, A Detailed Study of the Lucky Strike Hydrothermal Site and Discovery of a New Hydrothermal Site: Menez Gwen; Preliminary Results of the DIVA1 Cruise (5-24 May 1994): InterRidge News, v. 3, p. 14–17.

Fowler, A.P.G., Zierenberg, R.A., Schiffman, P., Marks, N., and Friðleifsson, G.Ó., 2015, Evolution of fluid-rock interaction in the Reykjanes geothermal system, Iceland: Evidence from Iceland Deep Drilling Project core RN-17B: Journal of Volcanology and Geothermal Research, v. 302, p. 47–63, doi: 10.1016/j.jvolgeores.2015.06.009.

Francis, T.J.G., 1973, The seismicity of the Reykjanes Ridge: Earth and Planetary Science Letters, v. 18, p. 119–123, doi: 10.1016/0012-821X(73)90042-3.

Franzson, H., Gunnlaugsson, E., Árnason, K., Sæmundsson, K., Steingrimsson, B., and Hardarson, B.S., 2010, The Hengill Geothermal System , Conceptual Model and Thermal Evolution, Proceedings of the 2010 World Geothermal Congress, Bali, Indonesia, 25-29 April, p. 25–29.

German, C.R., Briem, J., Chin, C., Danielsen, M., Holland, S., James, R., Jónsdóttir, A., Ludford, E., Moser, C., Ólafsson, J., Palmer, M.R., and Rudnicki, M.D., 1994, Hydrothermal activity on the Reykjanes Ridge: the Steinahóll vent-field at 63°06′N: Earth and Planetary Science Letters, v. 121, no. 3-4, p. 647–654, doi: 10.1016/0012-821X(94)90098-1.

German, C.R., Parson, L.M., and Team, H.S., 1996, Hydrothermal exploration near the Azores Triple Junction: tectonic control of venting at slow-spreading ridges?: Earth and Planetary Science Letters, v. 138, p. 93–104, doi: 10.1016/0012-821X(95)00224-Z.

Goslin, J., Lourenço, N., Dziak, R.P., Bohnenstiehl, D.R., Haxel, J., and Luis, J., 2005, Long-term seismicity of the Reykjanes Ridge (North Atlantic) recorded by a regional

hydrophone array: Geophysical Journal International, v. 162, p. 516–524, doi: 10.1111/j.1365-246X.2005.02678.x.

Gudmundsson, A., 1987, Geometry, formation and development of tectonic fractures on the Reykjanes Peninsula, southwest Iceland: Tectonophysics, v. 139, p. 295–308, doi: 10.1016/0040-1951(87)90103-X.

Hannington, M., Harðardóttir, V., Garbe-Schönberg, D., and Brown, K.L., 2016, Gold enrichment in active geothermal systems by accumulating colloidal suspensions: Nature Geoscience, v. 9, p. 299–303, doi: 10.1038/NGEO2661.

Hannington, M.D., Jamieson, J.W., Monecke, T., and Petersen, S., 2010, Modern seafloor massive sulfides and base metal resources: toward an estimate of global seafloor massive sulfide potential: Society of Economic Geologists Special Publication, v. 15, p. 317–338.

Haraldsdóttir, H.S., Franzson, H., and Árnason, K., 2012, Preliminary study of down-hole resistivity from 72 boreholes in the S-Hengill Geothermal Field, SW-Iceland, with respect to surface resistivity data and alteration minerals, *in* 37th Workshop on Geothermal Reservoir Engineering, Stanford University, Stanford, California, p. 10.

Head, W., Wilson, L., and Smith, D.K., 1996, Mid-ocean ridge eruptive vent morphology and substructure: Evidence for dike widths, eruption rates, and evolution of eruptions and axial volcanic ridges: Journal of Geophysical Research Solid Earth, v. 101, p. 28265–28280, doi: 10.1029/96JB02275.

Hey, R.N., Höskuldsson, A., Driscoll, N., and Dietrick, R., 2003, Marine Geophysical Investigations of Vestmannaeyjar and the Reykjanes Ridge, Iceland: Eos Transactions AGU, v. 84, p. F1521.

Höskuldsson, Á., Hey, R., Kjartansson, E., and Guðmundsson, G.B., 2007, The Reykjanes Ridge between 63°10′N and Iceland: Journal of Geodynamics, v. 43, p. 73–86, doi: 10.1016/j.jog.2006.09.003.

Hubbard, A., Sugden, D., Dugmore, A., Norddahl, H., and Peturssonc, H.G., 2006, A modelling insight into the Icelandic Last Glacial Maximum ice sheet: Quaternary Science Reviews, v. 25, p. 2283–2296, doi: 10.1016/j.quascirev.2006.04.001.

Ito, G., 2001, Reykjanes "V"-shaped ridges originating from a pulsing and dehydrating mantle plume: Nature, v. 411, p. 681–684, doi: 10.1038/35079561.

Jakobsdóttir, S.S., 2008, Seismicity in Iceland: 1994 – 2007: Jökull, , v. 58, p. 75–100.

Jakobsson, S.P., Jonsson, J., and Shido, F., 1978, Petrology of the Western Reykjanes Peninsula, Iceland: Journal of Petrology, v. 19, p. 669–705, doi: 10.1093/petrology/19.4.669.

Johannesson, H., 1980, Evolution of rift zones in western Iceland (in Icelandic with an English summary), Natturufraedingurinn, v. 50, p. 13–31.

Johannesson, H., 2014, Geological Map of Iceland: Bedrock Geology: [Map], 1: 600 000, Náttúruminjasafn Íslands, Reykjanvik.

Jónsson, J., 1978, Geological map of the Reykjanes Peninsula [in Icelandic]: Orkustofnun, Report and map, OS JHD 783, pp. 303.

Keeton, J.A., Searle, R.C., Parsons, B., White, R.S., Murton, B.J., Parson, L.M., Peirce, C., and Sinha, M.C., 1997, Bathymetry of the Reykjanes Ridge: Marine Geophysical Research, v. 19, p. 55–64, doi: 10.1023/A:1004266721393.

Khodayar, M., and Einarsson, P., 2002, Strike-slip faulting, normal faulting, and lateral dike injections along a single fault: Field example of the Gljúfurá fault near a Tertiary oblique rift-transform zone , Borgarfjörður, west Iceland: Journal of Geophysical Research, v. 107, p. 1–16, doi: 10.1029/2001JB000150.

Klein, F.W., Einarsson, P., and Wyss, M., 1977, The Reykjanes Peninsula, Iceland, earthquake swarm of September 1972 and its tectonic significance: Journal of Geophysical Research, v. 82, p. 865–888, doi: 10.1029/JB082i005p00865.

Langmuir, C., Humphris, S., Fornari, D., Van Dover, C., Von Damm, K., Tivey, M.K., Colodner, D., Charlou, J.-L., Desonie, D., Wilson, C., Fouquet, Y., Klinkhammer, G., and Bougault, H., 1997, Hydrothermal vents near a mantle hot spot: the Lucky Strike vent field at 37°N on the Mid-Atlantic Ridge: Earth and Planetary Science Letters, v. 148, p. 69–91, doi: 10.1016/S0012-821X(97)00027-7.

Leroy, S., D'Acremont, E., Tiberi, C., Basuyau, C., Autin, J., Lucazeau, F., and Sloan, H., 2010, Recent off-axis volcanism in the eastern Gulf of Aden: Implications for plume – ridge interaction: Earth and Planetary Science Letters, v. 293, p. 140–153, doi: 10.1016/j.epsl.2010.02.036.

Lilwall, R.C., Francis, T.J.G., and Porter, I.T., 1980, Some ocean-bottom seismograph observations on the Reykjanes Ridge at 59°N: Geophysical Journal International, , no. 62, p. 321–327, doi: 10.1111/j.1365-246X.1980.tb04858.x.

Litvin, V.M., 1984, The Structure of Sedimentary Series and its Role in the Morphostructure of the Ocean Floor, *in* Litvin, V.M. [Ed.], The Morphostructure of the Atlantic Ocean Floor, Springer Netherlands, p. 51–76, doi: 10.1007/978-94-009-6245-3.

Macdonald, K.C., Haymon, R.M., Blasius, J., and Benjamin, S., 2002, Off-axis Hydrothermal Activity on the East Pacific Rise near 9°28N: Faulted and Topographic Control of Hydrothermal Discharge?: AGU Abstract,.

Maochang, H., 2001, Possible environmental impacts of drilling exploratory wells for geothermal development in the Brennisteinsfjöll area, SW Iceland: Geothermal training program, Report 5/2001: The United Nations University, pp. 32.

Markússon, S.H., and Stefánsson, A., 2011, Geothermal surface alteration of basalts, Krýsuvík, Iceland -Alteration mineralogy, water chemistry and the effects of acid supply on the alteration process: Journal of Volcanology and Geothermal Research, v. 206, p. 46–59, doi: 10.1016/j.jvolgeores.2011.05.007.

Mawejje, P., 2007, Geothermal exploration and geological mapping at Seltun in Krysuvik Geothermal Field, Reykjanes Peninsula, SW Iceland, Report 12, p. 257–276.

Mochizuki, M., Brandsdóttir, B., Shiobara, H., Gudmundsson, G., Stefansson, R., and Shimamura, H., 2000, Detailed distribution of microearthquakes along the northern Reykjanes Ridge, off SW-Iceland: Geophysical Research Letters, v. 27, p. 1945–1948, doi: 10.1029/1999GL011264.

Murton, B.J., and Parson, L.M., 1993, Segmentation, volcanism and deformation of oblique spreading centres: a quantitative study of the Reykjanes Ridge: Tectonophysics, v. 222, p. 237–257, doi: 10.1016/0040-1951(93)90051-K.

Pałgan, D., Devey, C.W., and Yeo, I.A., 2016, Dike control of hydrothermal circulation in the Tertiary Icelandic crust and implications for cooling of the seafloor: Journal of Volcanology and Geothermal Research, v. 316, p. 22–33, doi: 10.1016/j.jvolgeores.2016.02.021.

Parson, L.M., Murton, B.J., Searle, R.C., Booth, D., Evans, J., Field, P., Keeton, J., Laughton, A., McAllister, E., Millard, N., Redbourne, L., Rouse, I., Shor, A., Smith, D., et al., 1993, En echelon axial volcanic ridges at the Reykjanes Ridge: a life cycle of volcanism and tectonics: Earth and Planetary Science Letters, v. 117, p. 73–87, doi: 10.1016/0012-821X(93)90118-S.

Pedersen, G.B.M., and Grosse, P., 2014, Morphometry of subaerial shield volcanoes and glaciovolcanoes from Reykjanes Peninsula, Iceland: Effects of eruption environment: Journal of Volcanology and Geothermal Research, v. 282, p. 115–133, doi: 10.1016/j.jvolgeores.2014.06.008.

Pedersen, G.B.M., Höskuldsson, A., Dürig, T., Thordarson, T., Jónsdóttir, I., Riishuus, M.S., Óskarsson, B.V., Dumont, S., Magnusson, E., Gudmundsson, M.T., Sigmundsson, F., Drouin, V.J.P.B., Gallagher, C., Askew, R., et al., 2017, Lava field evolution and emplacement dynamics of the 2014–2015 basaltic fissure eruption at Holuhraun, Iceland: Journal of Volcanology and Geothermal Research, v. 340, p. 155–169, doi: 10.1016/j.jvolgeores.2017.02.027.

Peirce, C., Gardiner, A., and Sinha, M., 2005, Temporal and spatial cyclicity of accretion at slow-spreading ridges-evidence from the Reykjanes Ridge: Geophysical Journal International, v. 163, p. 56–78, doi: 10.1111/j.1365-246X.2005.02738.x.

Peirce, C., and Sinha, M.C., 2008, Life and death of axial volcanic ridges: Segmentation and crustal accretion at the Reykjanes Ridge: Earth and Planetary Science Letters, v. 274, p. 112–120, doi: 10.1016/j.epsl.2008.07.011.

Perfit, M.R., and Chadwick Jr., W.W., 1998, Magmatism at mid-ocean-ridges: constrains from volcanological and geochemical investigations, In: Buck, W.R., Delaney, P.T., Karson, J.A., and Lagabrielle, Y. [Eds.], Faulting and Magmatism at Mid-Ocean Ridges, American Geophysical Union, Washington D.C., p. 59–116, doi: 10.1029/GM106p0059.

Poore, H., White, N., and Maclennan, J., 2011, Ocean circulation and mantle melting controlled by radial flow of hot pulses in the Iceland plume: Nature Geosci., v. 4, p. 558–561, doi: 10.1038/ngeo1161.

Rossi, M.J., 1996, Morphology and mechanism of eruption of postglacial shield volcanoes in Iceland: Bulletin of Volcanology, v. 57, p. 530–540, doi: 10.1007/BF00304437.

Ruddiman, W.F., 1972, Sediment Redistribution on the Reykjanes Ridge: Seismic Evidence: Geological Society of America Bulletin, v. 83, p. 2039–2062, doi: 10.1130/0016-7606(1972)83[2039:SROTRR]2.0.CO;2.

Russell, J.K., Edwards, B.R., Porritt, L., and Ryane, C., 2014, Tuyas: a descriptive genetic classification: Quaternary Science Reviews, v. 87, p. 70–81, doi: 10.1016/j.quascirev.2014.01.001.

Sæmundsson, K., 1992, Geology of the Thingvallavatn Area: Oikos, v. 64, p. 40–68, doi: 10.2307/3545042.

Sæmundsson, K., 1979, Outline of the geology of Iceland: Jökull, v. 29, p. 7–28.

Sæmundsson, K., Johannesson, H., Hjartarson, Á., Kristinsson, S.G., and Sigurgeirsson, M.A., 2010, Geological Map of the Southwest Iceland, [Map], 1:100 000, Iceland GeoSurvey, Reykjavik.

Sauter, D.L.M., and Cannat, M., 2010, The ultraslow spreading Southwest Indian Ridge, in Rona, P., Devey, C. W., Dyment, J., and Murton, B., [Eds.], Diversity of hydrotehrmal systems on slow spreading ocean ridges, American Geophysical Union, Washington D.C., p. 153–173, doi: 10.1029/2008GM000843.

Searle, R.C., Field, P.R., and Owens, R.B., 1994, Segmentation and nontransform ridge offset on the Reykjanes Ridge near 58°N: Journal of Geophysical Research, v. 99, p. 159–172, doi: 10.1029/94JB01549.

Searle, R.C., Keeton, J.A., Owens, R.B., White, R.S., Mecklenburgh, R., and Parsons, B., 1998, The Reykjanes Ridge: structure and tectonics of a hot-spot-influenced, slow-spreading ridge, from multibeam bathymetry, gravity and magnetic investigations: Earth and Planetary Science Letters, v. 160, p. 463–478.

Sigmundsson, F., Hooper, A., Hreinsdóttir, S., Vogfjörd, K.S., Ófeigsson, B.G., Heimisson, E.R., Dumont, S., Parks, M., Spaans, K., Gudmundsson, G.B., Drouin, V., Árnadóttir, T., Jónsdóttir, K., Gudmundsson, M.T., et al., 2014, Segmented lateral dyke growth in a rifting event at Bárðarbunga volcanic system, Iceland: Nature, v. 517, p. 191–195, doi: 10.1038/nature14111.

Sigurgeirsson, M.A., 2004, Chapter in the eruptive history of the Reykjanes Peninsula, eruptive episode at 2000 years BP (in Icelandic): Natturufraedingurinn, v. 72, p. 21–28.

Sinha, M.C., Constable, S.C., Peirce, C., White, A., Heinson, G., Macgregor, L.M., and Navin, D.A., 1998, Magmatic processes at slow spreading ridges: implications of the RAMESSES experiment at 57°45'N on the Mid-Atlantic Ridge: Geophysical Journal International, v. 135, p. 731–745, doi: 10.1046/j.1365-246X.1998.00704.x.

Smith, D.K., and Cann, J., 1990, Hundreds of small volcanoes on the median valley floor of the Mid-Atlantic Ridge at 24–30° N: Nature, v. 348, p. 152–155, doi: 10.1038/348152a0.

Standish, J.J., and Sims, K.W.W., 2010, Young off-axis volcanism along the ultraslow spreading Southwest Indian Ridge: Nature Geoscience, v. 3, p. 286–292, doi: 10.1038/ngeo824.

Stefánsson, R., Böðvarsson, R., Slunga, R., Einarsson, P., Jakobsdóttir, S., Bungum, H., Gregersen, S., Havskov, J., Hjelme, J., and Korhonen, H., 1993, Earthquake prediction research in the South Iceland Seismic Zone and the SIL project: Seismol. Soc. Am. Bull., v. 83, no. 3, p. 696–716.

Talwani, M., Windisch, C.C., and Langseth, M.G., 1971, Reykjanes Ridge crest: A detailed geophysical study: Journal of Geophysical Research, v. 76, p. 473–577, doi: 10.1029/JB076i002p00473.

Thorarinsson, S., 1965, Nedansjavargos vid Island (Submarine eruptions around Iceland): Natturufraedingurinn, v. 35, p. 49–74.

Titarenko, S.S., and McCaig, A.M., 2015, Modelling the Lost City hydrothermal field: influence of topography and permeability structure: Geofluids, v. 16, p. 314–328, doi: 10.1111/gfl.12151.

Torfason, H., 2003, Geothermal Map of Iceland [Map], 1: 500 000, Náttúruminjasafn Íslands og Orkustofnun, Reykjavik.

Valdimarsson, H., and Malmberg, S., 1999, Near-surface circulation in Icelandic waters derived from satellite tracked drifters: Rit Fiskideildar, v. 16, p. 23–39.

Vogt, P.R., 1971, Asthenosphere motion recorded by the ocean floor south of Iceland: Earth and Planetary Science Letters, v. 13, p. 153–160, doi: 10.1016/0012-821X(71)90118-X.

Weir, N.R., White, R.S., Brandsdottir, B., Einarsson, P., Shimamura, H., Shiobara, H., and Team, R.F., 2001, Crustal structure of the northern Reykjanes Ridge and Reykjanes Peninsula, southwest Iceland: Journal of Geophysical Research, v. 106, p. 6347–6368, doi: 10.1029/2000JB900358.

Yeo, I.A., 2012, Detailed studies of mid-ocean ridge volcanism at the Mid-Atlantic Ridge (45°N) and elsewhere [PhD Thesis], Durham University, United Kingdom, pp. 299.

Yeo, I. A., Clague, D.A., Martin, J.F., Paduan, J.B., and Caress, D.W., 2013, Preeruptive flow focussing in dikes feeding historical pillow ridges on the Juan de Fuca and Gorda Ridges: Geochemistry, Geophysics, Geosystems, v. 14, p. 3586–3599, doi: 10.1002/ggge.20210.

Yeo, I.A., Devey, C.W., LeBas, T.P., Augustin, N., and Steinführer, A., 2016, Segment-scale volcanic episodicity: Evidence from the North Kolbeinsey Ridge, Atlantic: Earth and Planetary Science Letters, v. 439, p. 81–87, doi: 10.1016/j.epsl.2016.01.029.

Yeo, I.A., and Searle, R.C., 2013, High-resolution Remotely Operated Vehicle (ROV) mapping of a slow-spreading ridge: Mid-Atlantic Ridge 45°N: Geochemistry, Geophysics, Geosystems, v. 14, p. 1693–1702, doi: 10.1002/ggge.20082.

Highlights

- Formation of Axial Volcanic Ridges is more complex than previous models suggest
- Faults on the Reykjanes Ridge strike orthogonal to spreading direction
- Seamounts and fault densities reflect volcanic robustness of Axial Volcanic Ridges
- Steinahóll Vent Field occupies shallow eruptive fissure located between two faults